# ANALYTICAL DESIGN OF ENERGETICALLY PASSIVE MECHANISMS

By

Amanda Sutrisno

Thesis

Submitted to the Faculty of the

Graduate School of Vanderbilt University

in partial fulfillment of the requirements

for the degree of

MASTER OF SCIENCE

in

MECHANICAL ENGINEERING

December 16, 2023

Nashville, Tennessee

Approved:

David Braun, Ph.D.

Eric Barth, Ph.D.

Michael Goldfarb, Ph.D.

## ACKNOWLEDGMENTS

I am grateful to Dr. David Braun, Vanderbilt University, and the Department of Mechanical Engineering for providing me with the chance to conduct advanced research and obtain my graduate degree in a field that I am very enthusiastic about. I am also thankful for the assistance and knowledge given by my complete thesis committee, namely Dr. Eric Barth and Dr. Michael Goldfarb. In addition, I would like to thank my labmates for their extensive guidance and encouragement. And finally, I would like to thank my friends and family for all their love and support.

## TABLE OF CONTENTS


Page

**LIST OF TABLES** . . . . . **iv**

**LIST OF FIGURES** . . . . . **v**

**1 Overview** . . . . . **1**

1.1 Introduction and Motivation . . . . . 1
1.2 Organization of the Document . . . . . 2

**2 Manuscript: Analytical Design of Energetically Passive Mechanisms** . . . . . **3**

2.1 Abstract . . . . . 3
2.2 Introduction . . . . . 3
2.3 Methods . . . . . 5
2.3.1 Mechanism . . . . . 5
2.3.2 Task . . . . . 6
2.3.3 Inverse Design . . . . . 6
2.3.3.1 Computing the Potential Energy Function . . . . . 6
2.3.3.2 Decomposing the Potential Energy Function . . . . . 7
2.3.3.3 Designing the Desired Potential Energy Function . . . . . 8
2.4 1-degree-of-freedom Example . . . . . 9
2.5 Experimental Validation . . . . . 22
2.6 Discussion and Conclusion . . . . . 28

**References** . . . . . **32**

## LIST OF TABLES


| Table | | Page |
|---|---|---|
| 2.1 | Physical dimensions of the cylindrical magnets used in the CST simulation and subsequent experiments to implement the basis structure. . . . . | 11 |
| 2.2 | Number of magnets used to construct each individual basis structure for each task. Each basis structure possesses a symmetric distribution of magnets, with half the magnets being placed on each of the two opposite ends of the stator, respectively. . . . . | 24 |

## LIST OF FIGURES


Figure Page

2.1 1 degree-of-freedom basis functions and structures, corresponding potential energy functions, and structural variations corresponding to each potential energy function. (a) Basis function (red), and scaled and shifted variants (blue, green, yellow) corresponding to structural variations. (b) Design of the basis structures. The basis structures are composed of a rotating magnet, whereby the rotation angle $\theta$ is the single degree of freedom, which repels against stationary magnets placed at a particular angle. The potential energy of the system is at a maximum when the rotating magnet is as close to the stationary magnets as possible. (c) Basis structure variations to scale and shift the potential energy function. This is done by moving the stationary magnets, or adding or subtracting the magnets. . . 10

2.2 1d basis structure implementation and simulation results. (a) Top view of schematic diagram of magnet configuration. There are two rotating cylindrical magnets placed at an angle $\mathbf{x}$ with respect to the horizontal, and $2N$ stacked magnets which are stationary(stator), where $N$ is an integer. (b) CST simulation schematic showing direction of magnetization of each magnet in the basis structure, we assume all cylindrical shapes have the same magnitude of magnetization. (c) Resulting simulated magnetic field used to compute the total potential energy. (d) Plot of simulated potential energy as a function of rotor angle $\mathbf{x}$ and $2N$ stacked stationary magnets. (e) Peak of the potential energy function in (d) as a function of $N$ stacked magnets. Black dashed line indicates interpolated values obtained by curve-fitting. (f) Spread of fitted Gaussian function $\sigma$. To obtain an analytical expression of the numerically simulated potential energy in (d), we fitted a Gaussian function $ce^{-(x-x_0)^2/\sigma^2}$, where $c$ is the maximum value of the function, $x_0$ is the position the maximum occurs, and $\sigma$ is the spread of the function. The spread $\sigma$ is a measure of the width of the basis function. . . . . 12

2.3 Design pipeline to make a spring which decreases torque the further away it is displaced from equilibrium. (a) Task requirements formulated in terms of desired torque function (grey). (b) Desired torque function integrated to obtain desired potential energy function (grey). (c) Attempting to decompose the desired potential energy function in terms of a series expansion of basis functions, where the initial guess for the coefficients of each basis function are obtained from the value of desired potential energy where the maximum value of each individual basis function is located. (d) Final potential energy obtained by optimizing basis function coefficients and summing the resulting series expansion (black dashed). Individual basis function contributions are shown in colored dashed lines. (e) Final mechanical design translated from basis functions in prior step. This final design is composed of cylindrical magnets arranged on a static ring of various lengths. The position coordinate $x$ in the basis functions corresponds to the angular position of two rotating magnets in the center of the ring of stationary magnets. Direction of magnetiziation of each magnet is indicated by the blue arrows, each magnet has a constant and uniform magnetization equal in magnitude to all other magnets. (f) Simulated potential energy function of the magnet configuration from (e). This plot was obtained by numerically simulating the magnetic field of the system in (e) using CST software, while sweeping the rotor angle $x$ from $[0, \pi]$. . . . . 15

2.4 Design problem for a spring with three equilibrium lengths of equal potential energy, and the resulting basis function solution and final mechanical design. (a) Torque versus rotor angle $x$ plot of desired torque (grey), approximation using basis functions(black dashed), and individual basis functions in approximation (colored dashed). (b) Resulting magnetic configuration of final mechanism design. Grey rectangles are the top view of cylindrical magnets, while blue arrows indicate direction of magnetization. Each magnet has the same magnitude of magnetization, but with different directions. $x$ indicates the rotation angle of the center magnets, which are movable. (c) Potential energy vs. rotor angle $x$ of the integral of the desired torque (grey), the sum of the basis functions to approximate the integral of desired torque (black dashed), and the individual basis functions (colored dashed). (d) Simulation results of the potential energy vs. rotor angle $x$ of the magnet configuration in (b) found using CST software. . . . . 17

2.5 Design problem for a spring with three equilibrium lengths of different potential energy, and the resulting basis function solution and final mechanical design. (a) Torque vs. rotor angle $x$ plot of desired torque(grey), approximation using basis functions(black dashed), and individual basis functions in approximation(colored dashed). (b) Resulting magnetic configuration of final mechanism design. Grey rectangles are the top view of cylindrical magnets, while blue arrows indicate direction of magnetization. Each magnet has the same magnitude of magnetization, but with different directions. $x$ indicates the rotation angle of the center magnets, which are movable. (c) Potential energy vs. rotor angle $x$ of the integral of the desired torque(grey), the sum of the basis functions to approximate the integral of desired torque(black dashed), and the individual basis functions(colored dashed). (d) Simulation results of the potential energy vs. rotor angle $x$ of the magnet configuration in (b) found using CST software. . . . . 19

2.6 Adjustable spring mechanism made from eight 1-degree-of-freedom basis structures connected in parallel. (a,b,c) The spring consists of a rotor with magnets on both sides, and a cylindrical stator consisting of 16 magnet slots, i.e an individual basis structure, which can be reconfigured to vary the number of magnets to scale/shift the individual basis potential energy function. The torque-deflection of the spring is obtained by attaching a lever arm to the rotor via a set-srew attachment to the rotating shaft, and pressing on a loadcell attached to the lever arm to get force data, and using a magnetic rotary encoder to obtain position data. Because the stator magnets repel the rotor magnets, a slot door with m5 heated inserts and bolts are used to press the magnets inwards so they remain stationary. (d) Electronics used to process sensor data. An op-amp circuit and a low pass filter (resistor and capacitor) are used to amplify the loadcell signal and filter for noise, respectively, before the voltage is read by a microcontroller and sent to a desktop computer running simulink realtime. . . . . 21

2.7 Experimental data obtained of a single basis function. (a) Torque vs. rotor angle $x$ of 6 experimental trials (grey), the average of the experimental trials (blue), and the fitted Gaussian derivative function with respect to the average (black dashed). (b) Potential energy vs. rotor angle $x$ of the integral of 6 experimentally obtained torque-deflection curves (grey), the average of the 6 integrated torque-deflection curves (blue), and the fitted Gaussian potential function (black dashed). . . . . 23

2.8 Experimental setup for a 1-degree-of-freedom spring with magnets configured for a torque-deflection curve which decreases absolute torque as the distance from the equilibrium length increases. (a) Overhead view showing configuration of magnets and position of the rotor $\theta$. There are 8 positions which form the centers of the Gaussian potential basis functions, labeled "pos. 1" up to "pos. 8." (b) Measured torque-deflection curve, raw data(grey lines), average of raw data (blue line), sum of Gaussian fitted curves (black dashed line). (c) Torque-deflection curves of each individual Gaussian derivative curve (colored lines) in the fitted curve (black dashed line). (d) Potential energy function obtained from integrating measured(grey lines), integral of the average of measured torque(blue line), and integral of the fitted torque deflection curve(black dashed line). (e) Potential energy curves of each individual Gaussian curve (colored lines) in the fitted curve (black dashed line). These are the basis functions obtained by fitting to experimental data. . . . . 25

2.9 Experimental setup for a 1-degree-of-freedom spring with magnets configured for a torque deflection curve with three equilibrium lengths of equal potential energy. (a) Overhead view showing magnet configuration There are 8 positions which form the centers of the Gaussian potential basis functions, labeled "pos. 1" up to "pos. 8." (b) Measured torque-deflection curve, raw data (grey lines), average of raw data (blue line), sum of Gaussian fitted curves (black dashed line). (c) Torque-deflection curves of each individual Gaussian derivative curve (colored lines) in the fitted curve (black dashed line). (d) Potential energy function obtained from integrating measured (grey lines), integral of the average of measured torque(blue line), and integral of the fitted torque deflection curve (black dashed line). (e) Potential energy curves of each individual Gaussian curve (colored lines) in the fitted curve (black dashed line). These are the basis functions obtained by fitting to experimental data. . . . . 26

2.10 Experimental setup for a 1-degree-of-freedom spring with magnets configured for a torque deflection curve with three equilibrium lengths of different potential energies. (a) Overhead view showing magnet configuration There are 8 positions which form the centers of the Gaussian potential basis functions, labeled "pos. 1" up to "pos. 8." (b) Measured torque-deflection curve, raw data (grey lines), average of raw data (blue line), sum of Gaussian fitted curves (black dashed line). (c) Torque-deflection curves of each individual Gaussian derivative curve (colored lines) in the fitted curve (black dashed line). (d) Potential energy function obtained from integrating measured(grey lines), integral of the average of measured torque(blue line), and integral of the fitted torque deflection curve(black dashed line). (e) Potential energy curves of each individual Gaussian curve (colored lines) in the fitted curve (black dashed line). These are the basis functions obtained by fitting to experimental data. . . . . 27

# CHAPTER 1

# Overview

## 1.1 Introduction and Motivation

Passive mechanisms are devices which can perform a task without an internal power-source. Simple examples of such devices include a lever to amplify applied force via mechanical advantage, a spring to store and release energy at a specific frequency, or ice-skates and bicycles which allow humans to move faster. Not every task can be done using a passive mechanism, passive mechanisms are only feasible for cyclic tasks in which no net-work is done. Meanwhile, active mechanisms can be used to do any task, whether active or passive. However, if a task can be done using a passive mechanism, then it is advantageous over using an active mechanism because of potential energy cost savings and weight reduction due to lack of batteries.

The reason why active-mechanisms might be used for tasks which could instead be done using passive mechanisms is that active mechanisms are easier to design for a task. This is because active mechanisms are frequently composed of actuators, which are motors attached to a transmission mechanism which changes position when driven by the motor. In an active mechanism, the force that the actuators may exert can be programmed arbitrarily regardless of the position of the actuator. In contrast, passive mechanisms are composed of springs or springy mechanisms attached to a transmission mechanism, where the force exerted is a fixed function of the position of the mechanism. Therefore, passive mechanisms for one task may not be re-usable for other tasks if they require different functions of force relative to position/deflection. Furthermore, it may not even be certain what force is required at which position, unlike when using an active mechanism where the required force can be found using feedback control, and programmed accordingly during motion. Therefore, this poses a difficult two-part design problem for passive mechanisms where first a suitable force-deflection curve has to be found to complete a task, and next an appropriate mechanical structure has to be found that embodies that force-deflection curve. Furthermore, a task may require more than one degree of freedom, such that the force-deflection curve is a vector valued function which further complicates the design algorithm.

To alleviate the difficulty of designing passive mechanisms, optimization methods, particularly topology-optimization can be used. Topology optimization is when an optimization problem is formulated in which the optimization variable is a mechanical template structure which may vary in shape, and the objective function is how well the structure achieves the task. Originally, topology optimization was applied to simple load bearing tasks where the task is to hold up a certain load with as little mass in the mechanical structure

as possible. Further extensions of topology optimization were to create transmission mechanisms where an input degree of freedom would move at a constant rate of deflection, while an output degree of freedom would trace a separate curve as a function of the input degree of freedom. In theory, any task can be formulated as a topology optimization problem in order to find a passive mechanism. However, we note that topology optimization has limitations in finding a feasible solution, because it is i) dependent on the choice of a correct template, ii) dependent on a close enough initial guess, and iii) is not guaranteed to find the optimal mechanism unless the problem is mathematically convex, which is difficult to prove except for the simplest problems.

A topology optimization problem is one attempt at solving the larger design problem by turning the design problem into a math problem, and using an approximate numerical tool to solve the said mathematical problem. If there were an analytical rather than numerical method of solving the same problem, then one could explore guarantees for the existence of the design. In this thesis, we propose an analytical design method for a particular problem formulation of designing passive mechanisms. This method exploits the fact that passive mechanisms are by nature energetically conservative, such that an entirely state-dependent (rather than path dependent) potential energy function can be written as a function of the positions of the degrees of freedom of the mechanism. Furthermore, many mathematical functions can be decomposed into a series expansion of basis functions. We then design mechanical structures which have potential energy functions corresponding to mathematically complete local basis functions, which have variable internal parameters that can scale/shift these local basis functions to create other basis functions to form a mathematically complete set. These basis structures can then be connected in parallel to add their respective potential energy functions, which is mathematically equivalent to summing basis functions to form any desired potential energy function. Therefore, we present a pipeline of an algorithm to analytically solve a passive mechanism design problem, provided the passive mechanism to fulfill a task can be described in terms of a potential energy function.

### 1.2 Organization of the Document

This thesis is organized into two distinct chapters. Chapter 1 introduces the motivation of this work, while Chapter 2 presents the body of this work, consisting of the literature review, foundational theory, prototype design, simulation, and experimental validation for three example passive mechanism design problems.

# CHAPTER 2

## Manuscript: Analytical Design of Energetically Passive Mechanisms

Amanda Sutrisno and David J. Braun

Vanderbilt University

Nashville, Tennessee

### 2.1 Abstract

Energetically passive devices are rigid and complaint mechanisms that can amplify force as well as store and release energy with specific timings and forces. Designing a compliant mechanism for a given task, i.e "inverse design" of unpowered mechanisms, can be done numerically using topology optimization. However, topology optimization is computationally intensive and time consuming, and may not be guaranteed to find a near optimal design. Here we use approximation theory and the property that compliant mechanisms can be modeled by a scalar potential energy function to provide an approximate analytical solution to the inverse design of passive mechanisms. Using the proposed method, we created novel multi-stable mechanical structures which can (i) store energy like a spring with an unusual torque-deflection curve that decreases as the deflection angle is increased, (ii) store energy like a spring that has three equilibrium lengths of equal potential energy like three valleys of the same depth, and (iii) store energy like a spring but with three equilibrium lengths of increasing potential energy like a staircase.

### 2.2 Introduction

Energetically passive devices can manipulate force and energy in intelligent ways without requiring external power. Examples include the bicycle that allows humans to move faster, a wheel that automatically changes shape in response to applied torque [1], or springy legged robots that can walk, jump, or run with no energy input [2, 3, 4, 5, 6, 7]. More exotic examples of passive mechanical structures are meta-materials which can change shape and mechanical properties, for example the force response to deformation [8, 9, 10, 11, 12], and mechanical computers responding to the environment [13, 14]. These examples illustrate that complex tasks can be performed using devices that require no power provided a suitable mechanism can be designed [15, 16].

The exponential rise in computing power and artificial intelligence capability has attracted significant

interest in the field of "automatic (inverse) design", where high performance computing and sophisticated algorithms can aid human designers in creating new technologies. Prior attempts to automatically design passive mechanisms include industry-standard topology optimization algorithms used to optimize simple templates of continuum structures [17, 18, 19, 20, 21] and smart search algorithms that mix templates of discrete rigid and continuum structures [22, 23, 24, 25]. In both cases, a template structure – continuous or discrete – consisting of connected beams with variable lengths and thicknesses are adjusted until the behavior of the mechanical structure becomes reasonably close to the desired behavior of the structure subject to an external stimuli. Regardless of the template, the process of finding and simulating the desired structure is computationally intensive and time consuming, since the optimization problem to solve is usually large-scale and non-convex, leaving the designer with heuristic methods and no formal guarantees to find a near optimal design.

Here, we propose an alternative method to analytically compute a passive mechanical structure to fulfill a user defined task. We assume the task is energetically conservative, i.e requires no net mechanical energy, and the mechanical structure possesses finitely many degrees of freedom. The proposed analytical design method is composed of three main steps:

(1) In the first step, we compute a potential energy function consistent with the task defined by the input output relation between the force response of the mechanical structure under the effect of position changes along the desired work cycle. In this step, we leverage the fact that all energetically passive mechanisms can be mathematically represented by a potential energy function – a smooth scalar function which depends on the position inputs that coincide with the degrees of freedom of the mechanism.

(2) In the second step, we approximate the potential energy function that encodes the task with a sum of simpler functions that form a set of basis functions for the potentially complex desired potential energy function. In this step, we leverage the fact that smooth energy functions can be approximately represented by a sum of finitely many smooth basis functions.

(3) Finally, in the third step, we convert the sum of basis functions into a mechanical design by converting each term in the sum of basis functions into an individual mechanical structure, and connecting these structures in parallel to sum their potential energies.

The centerpiece of the proposed design procedure is a single template mechanical structure which possesses a localized potential energy function that can be shifted and scaled by varying a small number of physical parameters. This simple mechanical structure can then be replicated, shifted, scaled, and connected in parallel to each other to approximate complex potential energy functions representing a user defined task.

Using the proposed analytical inverse design methodology, we created three novel mechanical structures. The first structure can store energy like a spring, but possesses a torque which decreases as the deflection

is increased. The second structure also stores energy like a spring, but possesses three distinct equilibrium lengths with equal potential energy, with a large potential energy barrier in between adjacent equilibrium lengths. And finally, the last structure also stores energy and possesses three equilibrium lengths like the previous structure, but has a different potential energy at each equilibrium length. This allows the structure to retain energy even after the force applied to the structure is removed, similar to how a staircase allows "resting" while retaining gravitational potential energy. To accomplish the aforementioned tasks, we provide mechanical structures with mathematically complete local potential energy functions for 1-degree-of-freedom systems. The proposed inverse-design method may be extended to fulfill tasks requiring higher numbers of degrees of freedom, given that a mechanical structure can be found with adjustable physical dimensions to form mathematically complete potential energy functions.

## 2.3 Methods

In this section, we shall describe how to i) mathematically model a passive mechanism (Section 2.3.1), ii) mathematically model an energetically conservative task (Section 2.3.2), and iii) design a mechanism that can achieve the task (inverse design, Section 2.3.3).

### 2.3.1 Mechanism

We consider mechanical structures, i.e energetically passive mechanisms, with finitely many degrees of freedom. We assume the configuration of the mechanism is described by $N$ position coordinates,

$$\boldsymbol{x} = (x_1, x_2, ..., x_N) \in \Omega \subset \mathbb{R}^n, \tag{2.1}$$

where $\Omega$ is a closed and bounded set.

The mathematical model of the mechanisms is then given by a potential energy function – which is a twice continuously differentiable scalar function of the position coordinates:

$$V(\boldsymbol{x}). \tag{2.2}$$

Next we recall that energetically conservative mechanisms do no net mechanical work along any closed path, which implies the forces exerted by the mechanism are fully defined by the potential energy function, and can be calculated using the following formula:

$$\boldsymbol{F}(\boldsymbol{x}) = -\frac{\partial V(\boldsymbol{x})}{\partial \boldsymbol{x}}. \tag{2.3}$$

### 2.3.2 Task

The task is to move the mechanism along a path with a specified force. We assume that the path is closed, has finite length, and that the state of the mechanism along the path is defined by the following normalized path length coordinate $s \in [0,1] \in \mathbb{R}$. Consequently, the closed path can be represented by:

$$\boldsymbol{x}^*(s) \quad \text{and} \quad \boldsymbol{x}^*(0) = \boldsymbol{x}^*(1), \tag{2.4}$$

or the following equation:

$$\Phi(\boldsymbol{x}^*) = 0. \tag{2.5}$$

Aside from the path, the forces exerted by the structure moving along the path are also defined as part of the task. These forces are given by:

$$\boldsymbol{F}^*(s) = \boldsymbol{F}^*(\boldsymbol{x}^*(s)). \tag{2.6}$$

### 2.3.3 Inverse Design

In this section we shall convert the task requirements into a design using an analytical method. This method consists of i) converting the task requirements into a suitable potential energy function, ii) approximating the potential energy function using a series expansion of simpler functions, and iii) converting the simpler functions in the series expansion to simple mechanical structures that are connected in parallel to provide the desired final design.

#### 2.3.3.1 Computing the Potential Energy Function

In order to design a passive mechanism, we shall first compute a candidate potential energy function that guarantees stability of the desired path along which the mechanism exerts the desired forces. This can be done using the following three conditions:

$$-\frac{\partial V(\boldsymbol{x})}{\partial \boldsymbol{x}}\bigg|_{\boldsymbol{x}=\boldsymbol{x}^*(s)} = \boldsymbol{F}^*(s), \tag{2.7}$$

$$\forall \delta\boldsymbol{x}, \delta\boldsymbol{x}_\perp \text{ such that } \boldsymbol{x}^* + \delta\boldsymbol{x} \in \Omega,\ \boldsymbol{x}^* + \delta\boldsymbol{x}_\perp \in \Omega \text{ and } \delta\boldsymbol{x} \cdot \delta\boldsymbol{x}_\perp = 0 : -\frac{\partial V(\boldsymbol{x})}{\partial \boldsymbol{x}}\bigg|_{\boldsymbol{x}=\boldsymbol{x}^*(s)} \cdot \delta\boldsymbol{x}_\perp = 0, \tag{2.8}$$

and

$$\forall \delta \boldsymbol{x}, \delta \boldsymbol{x}_{\perp} \neq \mathbf{0} \text{ such that } \boldsymbol{x}^* + \delta \boldsymbol{x} \in \Omega, \ \boldsymbol{x}^* + \delta \boldsymbol{x}_{\perp} \in \Omega \text{ and } \delta \boldsymbol{x} \cdot \delta \boldsymbol{x}_{\perp} = 0 : (\delta \boldsymbol{x}_{\perp})^{\top} \frac{\partial^2 V(\boldsymbol{x})}{\partial \boldsymbol{x}^2}\bigg|_{\boldsymbol{x}=\boldsymbol{x}^*(s)} \delta \boldsymbol{x}_{\perp} > 0. \tag{2.9}$$

where $\delta \boldsymbol{x}$ is the vector tangent to the path defined by $\Phi(\boldsymbol{x}^*) = 0$, and $\delta \boldsymbol{x}_{\perp}$ is the vector perpendicular to the path as denoted by $\delta \boldsymbol{x} \cdot \delta \boldsymbol{x}_{\perp} = 0$. The first condition (2.7) indicates that the force exerted by the device along the desired path is equal to the desired force. The second (2.8) condition is necessary for the potential energy function to have an minimum in the plane perpendicular to the path. We note that stability of the path is not implied by this condition. The third condition (2.9) ensures that the path is locally stable in the plane perpendicular to the path, as it implies that the potential energy function rapidly increases along the $\delta \boldsymbol{x}_{\perp}$ away from $\boldsymbol{x}^*$, and has a minimum along the desired path when considered in the plane perpendicular to the path.

We note that there may be infinitely many potential energy functions that satisfy (2.7)-(2.9). Furthermore, each potential energy function is task-dependent and generally scales in complexity relative to the task complexity. Next we explore the decomposition of the task-dependent potential energy function into a sum of simpler functions independent of the task.

#### 2.3.3.2 Decomposing the Potential Energy Function

We conjecture that an arbitrarily complex energetically passive mechanical structure, may be decomposed into infinitely many structures connected in parallel. Based on this conjecture, we assume, that the potential energy function $V(\boldsymbol{x})$ of an arbitrarily complex energetically passive mechanical structure may be approximated by a finite series of potentially simpler functions $\{V_i(\boldsymbol{x})\}_{i=1}^{n}$. On the other hand, any smooth potential energy function can be represented by an infinite series of basis functions $\{\phi_i(\boldsymbol{x})\}_{i=1}^{\infty}$ spanning the space of smooth functions:

$$V(\boldsymbol{x}) = \sum_{i=1}^{\infty} V_i(\boldsymbol{x}) \approx \sum_{i=1}^{n} V_i(\boldsymbol{x}) = \sum_{i=1}^{n} c_i \phi_i(\boldsymbol{x}). \tag{2.10}$$

where $c_i$ denotes the contribution of the $\phi_i(\boldsymbol{x})$ basis function.

Given a set of ortho-normal basis functions $\int_{\Omega} \phi_i(\boldsymbol{x}) \phi_j(\boldsymbol{x}) dx = \delta_{ij}$, where $\delta_{ij}$ denotes the Kronecker delta symbol, the contribution of each individual basis function is defined by:

$$c_i = \int_{\Omega} V(\boldsymbol{x}) \phi_i(\boldsymbol{x}) dx. \tag{2.11}$$

Relations (2.10) and (2.11) associate each component in the decomposition of the potential energy functions with one basis function:

$$V_i(\boldsymbol{x}) = c_i \phi_i(\boldsymbol{x}). \tag{2.12}$$

Any basis function could serve to decompose the potential energy function in (2.10), however, not all basis functions will define potential energies (2.12) that can be easily converted into a mechanical structure.

In this paper we consider the class of compactly supported radial basis functions. An example of such function for a 1-degree-of-freedom system is given by:

$$\phi_i(\boldsymbol{x}) = \begin{cases} \frac{A}{2}\cos\left(\frac{x-x_{0i}}{\sigma}\right) + \frac{A}{2} & \text{if} \quad x_{0i} - \sigma\pi < x < x_{0i} + \sigma\pi \\ 0 & \text{otherwise.} \end{cases} \tag{2.13}$$

where $A$ is the maximum value of the function, $x_{0i}$ is the $x$ position where the maximum value occurs, and $2\pi\sigma$ determines the width of the Gaussian function where it is nonzero.

These type of functions can be used to approximate the potential energy function uniformly in the space of smooth function; such that both the forces and the stiffness of the structure can be made arbitrarily close to their exact values by increasing the number of terms in (2.10). We further note that for non-negative potential energy functions $\forall \boldsymbol{x} \in \Omega : V(\boldsymbol{x}) \geq 0$, the basis functions above guarantee that each individual potential energy function is a non-negative function,

$$\forall \boldsymbol{x} \in \Omega : V_i(\boldsymbol{x}) = c_i \phi_i(\boldsymbol{x}) \geq 0. \tag{2.14}$$

Because potential energy functions $\forall \boldsymbol{x} \in \Omega : V(\boldsymbol{x}) \geq 0$ form an equivalence class of functions which differ by a constant, the above relation can be satisfied with no restriction on generality.

Next we attempt to convert the potential energy function to a mechanical design.

#### 2.3.3.3 Designing the Desired Potential Energy Function

We are concerned with the design of one single parameterized mechanical structure that may be used to represent different potential energy functions defined by:

$$V_i(\boldsymbol{x}) = V(\boldsymbol{x}; c_i, \sigma_i, \boldsymbol{x}_{0i}) = c_i \phi(\sigma_i(\boldsymbol{x} - \boldsymbol{x}_{0i})). \tag{2.15}$$

This potential energy function has the same functional form, given by the same basis function $\phi$, but aside from the scaling with a non-negative number $c_i$, changing the center of the basis function $\boldsymbol{x}_{0i} \in \Omega$ provides

shifting, while changing $\sigma_i$ provides radial scaling.

We seek a mechanical structure that possesses at least $\boldsymbol{p} = (p_1, p_2, ..., p_{N+2}, ...) \in \mathbb{R}^{\geq N+2}$ physical parameters which can be varied to alter the potential energy function by scaling and shifting:

$$c_i = c(\boldsymbol{p}_i) \geq 0, \quad \sigma_i = \sigma(\boldsymbol{p}_i) \geq 0, \quad \text{and} \quad \boldsymbol{x}_{0i} = \boldsymbol{x}_0(\boldsymbol{p}_i) \in \Omega. \tag{2.16}$$

These mappings must be invertible, such that for any desired scaling $c_i, \sigma_i$, and shifting $\boldsymbol{x}_{0i}$, a set of mechanical design parameters $\boldsymbol{p}_i$ satisfying (2.16) can be computed, and a mechanical structure can be created. Relation (2.16) established the connection between the parameters of the potential energy functions computed for the desired task (2.15), and the physical dimensions of a mechanical structure $\boldsymbol{p}$.

Using the same mechanical structure with different physical dimensions that allow us to scale and shift the potential energy representation of each structure in the composition, we can rewrite the series expansion in (2.10) as the sum of the following potential energy functions,

$$V_i(\boldsymbol{x}) = V(\boldsymbol{x}; \boldsymbol{p}_i) = c(\boldsymbol{p}_i)\phi(\sigma(\boldsymbol{p}_i)(\boldsymbol{x} - \boldsymbol{x}_0(\boldsymbol{p}_i))). \tag{2.17}$$

In the next section we present a simple mechanical structure to exemplify the theory presented in this section for a 1-degree-of-freedom system.

### 2.4 1-degree-of-freedom Example

This section describes a proposed 1-degree-of-freedom basis structure and associated potential energy basis function, and a few 1-degree-of-freedom design problems. Furthermore, we carefully illustrate the mathematical procedure for analytically computing how to fine-tune multiple basis-structures to fit a desired potential energy function. The basis structures we present are composed of permanent magnets, and the resulting potential energy is only due to energy stored in magnetic fields. Therefore, we simulated the basis structure and the final mechanisms using magnetostatic simulations in CST Studio simulation software. We then designed a prototype and conducted experiments to collect torque-deflection data of the basis structure and the complete mechanisms, and integrate the torque-deflection curves to obtain potential energy functions.

Figure 2.1abc. shows the mechanical basis structure for a 1-degree-of-freedom system. Figure 2.1a. shows the potential energy basis functions, which appear as a Gaussian-like function. This basic Gaussian shape (red line) may be scaled (blue, green) and shifted (yellow) by structural variations, which will be explained later in Fig. 2.1bc. Figure 2.1b. shows the basis structure, which consists of a rotating arm with a magnet attached to one side which repels another magnet placed on a static outer ring, where the single degree

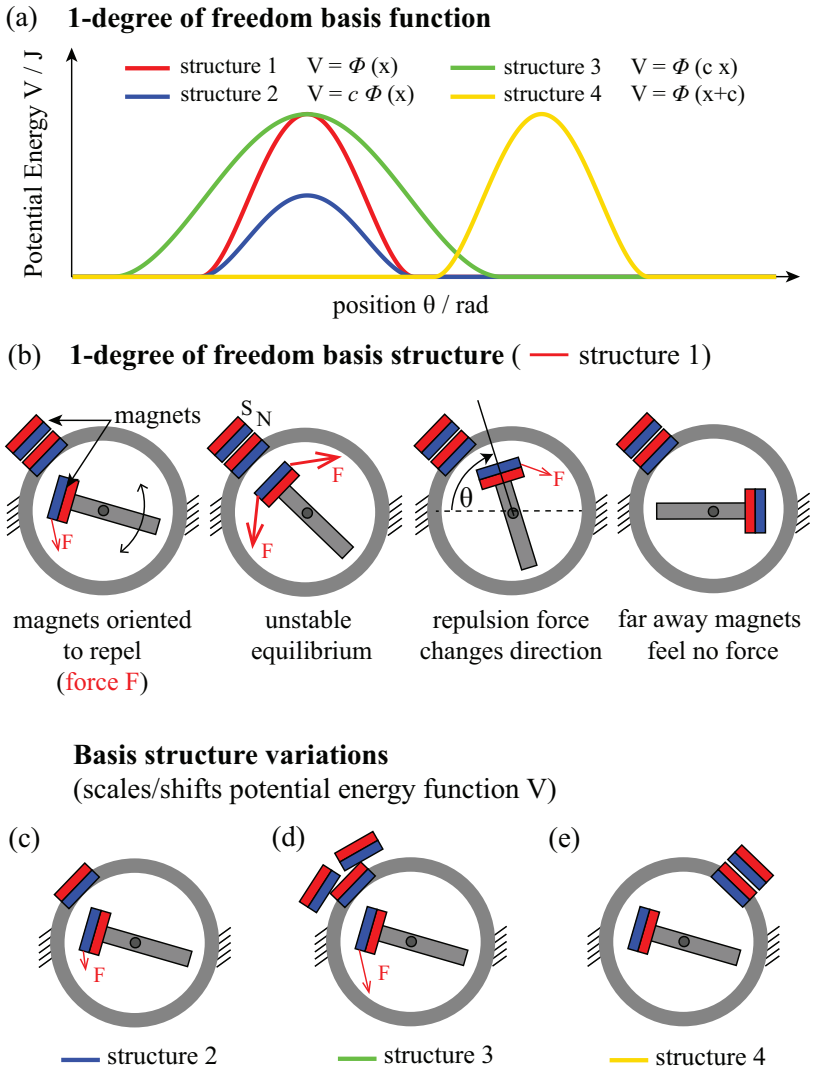


Figure 2.1: 1 degree-of-freedom basis functions and structures, corresponding potential energy functions, and structural variations corresponding to each potential energy function. (a) Basis function (red), and scaled and shifted variants (blue, green, yellow) corresponding to structural variations. (b) Design of the basis structures. The basis structures are composed of a rotating magnet, whereby the rotation angle $\theta$ is the single degree of freedom, which repels against stationary magnets placed at a particular angle. The potential energy of the system is at a maximum when the rotating magnet is as close to the stationary magnets as possible. (c) Basis structure variations to scale and shift the potential energy function. This is done by moving the stationary magnets, or adding or subtracting the magnets.

| description | symbol | unit | value |
|---|---|---|---|
| magnet radius | $r_{mag}$ | mm | 10 |
| magnet thickness | $h_{mag}$ | mm | 3 |
| magnetization | - | Wb | 0.895 |
| rotor radial distance | $r_{\text{rotor}}$ | mm | 53 |
| stator radial distnace | $r_{\text{stator}}$ | mm | 70.5 |

Table 2.1: Physical dimensions of the cylindrical magnets used in the CST simulation and subsequent experiments to implement the basis structure.

of freedom corresponds to the rotation angle $\theta$ of the rotor. The maximum potential energy, corresponding to the peak of the Gaussian potential function, occurs when the rotor magnet is aligned as closely as possible with the stator magnet. In Fig. 2.1c., we show how the physical parameters of the system can be varied to scale or shift the potential energy function. This is done by stacking more or less magnets in the stator, which scales the peak of the basis function, or distributing the stator magnets over a larger area, which scales the width of the basis function. And finally we can also keep the number of stator magnets constant but move them to a different position, which shifts the entire basis function with respect to the degree of freedom.

Figure 2.2 shows the schematic diagram for the simulation and subsequent experiment that implements the basis structure shown in Fig. 2.1. The dimensions of the magnets and how they are placed in this simulation and subsequent experiments are given by Table 2.1. Figure 2.2a. shows the schematic of the basis function, which consists of two inner rotating cylindrical magnets at an angle $\mathbf{x}$ with respect to the horizontal, and $2N$ outer magnets which form two separate stacks of $N$ magnets each which are stationary. Figure 2.2b shows the implementation of the simulation in CST software, where four cylinders are drawn with the same magnitude of magnetization but different directions of magnetization (blue arrows). Furthermore, we sweep the angle of the inner magnets about the z axis, and compute the resulting magnetic field at every different angle, shown in Fig. 2.2, which the CST software uses to compute total potential energy. The magnitude of magnetization of the magnets is not known before-hand, but only scales the total potential energy stored in the magnetic field quadratically, such that we can adjust this parameter until it agrees with the subsequent experiment data on a single basis structure. Figure 2.2d. shows the numerically computed potential energy as a function of rotor angle $x$ and $2N$ stacked magnets in the stator. To obtain an analytical expression of the potential energy as a function of system parameters, we fit a Gaussian function to the numerically computed potential energy function in Fig. 2.2d., which are shown in Fig. 2.2f., where the equation of the fitted functions are

$$V_i(x) = c_i e^{-\left(\frac{(x-x_{0i})}{\sigma_i}\right)^2}, \tag{2.18}$$

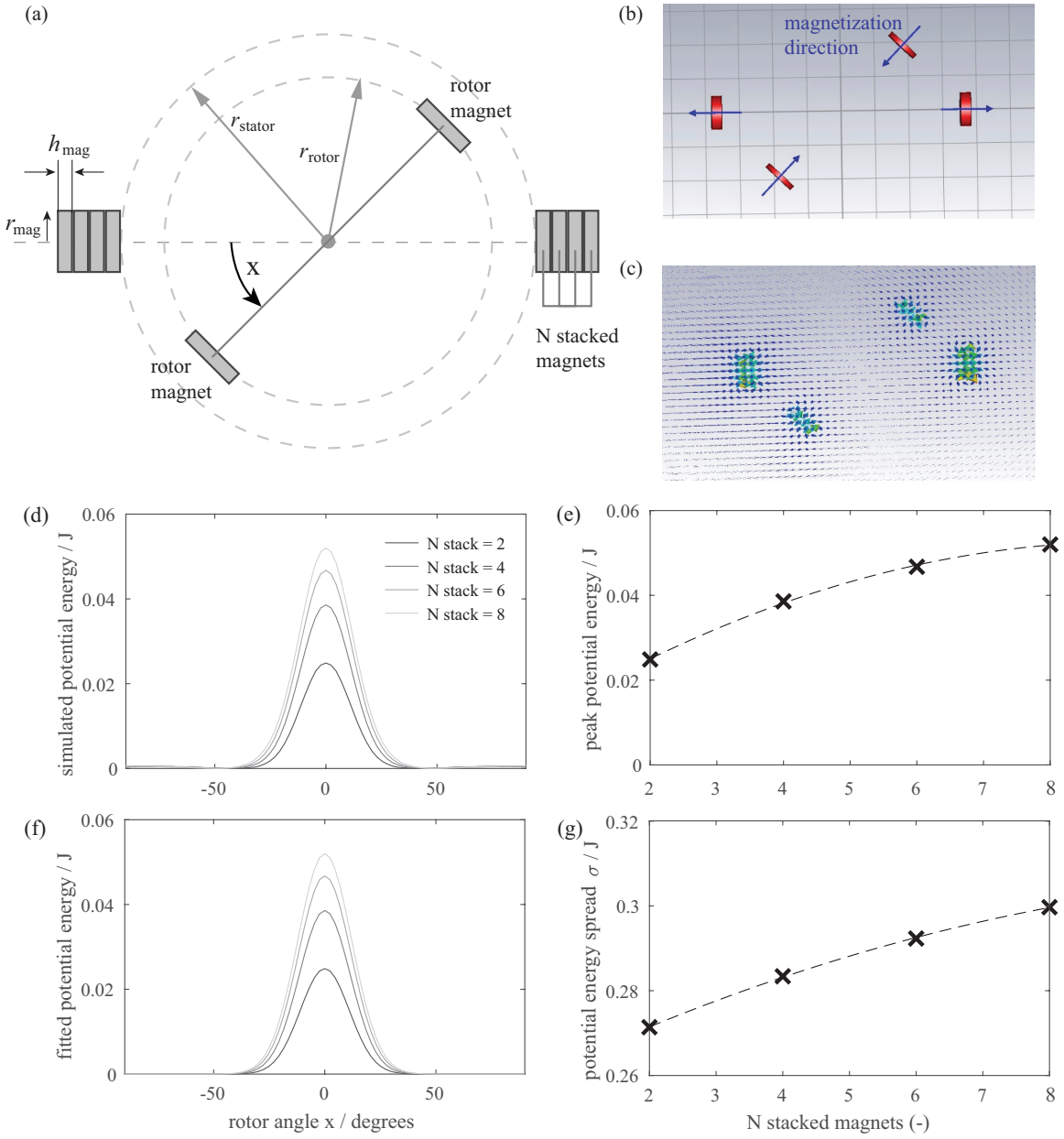


Figure 2.2: 1d basis structure implementation and simulation results. (a) Top view of schematic diagram of magnet configuration. There are two rotating cylindrical magnets placed at an angle **x** with respect to the horizontal, and 2$N$ stacked magnets which are stationary(stator), where $N$ is an integer. (b) CST simulation schematic showing direction of magnetization of each magnet in the basis structure, we assume all cylindrical shapes have the same magnitude of magnetization. (c) Resulting simulated magnetic field used to compute the total potential energy. (d) Plot of simulated potential energy as a function of rotor angle **x** and 2$N$ stacked stationary magnets. (e) Peak of the potential energy function in (d) as a function of $N$ stacked magnets. Black dashed line indicates interpolated values obtained by curve-fitting. (f) Spread of fitted Gaussian function $\sigma$. To obtain an analytical expression of the numerically simulated potential energy in (d), we fitted a Gaussian function $ce^{-(x-x_0)^2/\sigma^2}$, where $c$ is the maximum value of the function, $x_0$ is the position the maximum occurs, and $\sigma$ is the spread of the function. The spread $\sigma$ is a measure of the width of the basis function.

where

$$
\begin{aligned}
c_i &= 0.00761 + 0.00976 p_{i1} - 0.00052804 p_{i1}^2 \\
x_{0i} &= \frac{\pi}{8} p_{i2} \\
\sigma_i &= 0.257 + 0.00758 p_{i1} - 0.000289 p_{i1}^2 \\
p_{i1} &= \text{N stacked magnets} \in \{0,1,2,3,4,5,6,7,8\} \\
p_{i2} &= i \in \{0,1,2,3,4,5,6,7\}.
\end{aligned} \tag{2.19}
$$

According to (2.18) the simulated potential energy function of the basis structure is approximately Gaussian, with a maximum peak $c_i$, angular position the peak occurs $x_{0i}$, and spread $\sigma_i$ which varies with the parameters $p_{i1}, p_{i2}$, which are the number of stacked magnets and nth basis function $i$, respectively, shown in (2.19). Figure 2.2eg plots the analytical expressions for $c_i$ and $\sigma_i$ in (2.19), respectively, as a function of $p_{i1}$, or $N$ stacked magnets (black dashed lines). The procedure used to obtain the equations in (2.19) was to first simulate the potential energy function numerically in CST as a function of position, then fit the Gaussian function in (2.18) by adjusting $c_i, x_{0i}, \sigma_i$. Afterwards, we plot $c_i, x_{0i}, \sigma_i$ as a function of $N$, the number of stacked stator magnets, and fit a quadratic polynomial to obtain the relationship between $c_i, x_{0i}, \sigma_i$ and $N$, which we denote as $p_{i1}$.

Here we demonstrate how the analytical design method can be used to solve three specific design problems. However, we must first define a few constraints on the physical design. There are 8 possible unique positions for the magnets to be arranged on the stator, and therefore there are a maximum of 8 unique basis functions with their peaks shifted $\pi/8$ radians apart from each other. Each stator position can have a stack of magnets ranging from 1 to 8 stacked magnets, with only integer numbers in between due to experimental constraints. In the next few paragraphs, we shall detail the design problems. For simplicity, we supply the corresponding torque and potential energy functions which fulfills the design requirements, and then show how to embody that potential energy function by adjusting the physical parameters of the basis structures and connecting them in parallel.

(i) Design problem 1: A spring with decreasing torque deflection behavior.

The goal is to design a 1-degree-of-freedom spring with one equilibrium position, where the torque decreases the further the spring is displaced from equilibrium. The desired torque function which fulfills the design requirements is given by

$$\tau_d(x) = \begin{cases} -0.0535x & \text{if} \quad x < \frac{\pi}{2} - 0.17 \\ 0.441x - 0.693 & \text{if} \quad \frac{\pi}{2} - 0.17 \leq x \leq \frac{\pi}{2} + 0.17 \\ -0.0535x + 0.168 & \text{if} \quad x > \frac{\pi}{2} + 0.17. \end{cases} \tag{2.20}$$

This function (2.20) is visualized in Fig. 2.3a.

The next step is to integrate this torque function to obtain a desired potential energy function shown in Fig. 2.3b,

$$V_d(x) = \begin{cases} -0.0268x^2 + 0.06 & \text{if} \quad x < \frac{\pi}{2} - 0.17 \\ 0.221x^2 - 0.693x + 0.545 & \text{if} \quad \frac{\pi}{2} - 0.17 \leq x \leq \frac{\pi}{2} + 0.17 \\ -0.0268x^2 + 0.168x - 0.204 & \text{if} \quad x > \frac{\pi}{2} + 0.17. \end{cases} \tag{2.21}$$

We then take the desired potential energy function in (2.21), and approximate it using a sum of basis functions

$$V_d(x) \approx V(x) = \sum V_i(x) = \sum_{i=0}^{7} c_i e^{-\frac{(x-x_{i0})^2}{\sigma_i^2}}. \tag{2.22}$$

Then we formulate an optimization problem which finds the physical parameters $p_{i1}$, or the number $N$ stacked magnets in each basis structure for $i = 0, 1, 2, ..., 7$ that minimizes the difference between the desired potential energy function and the potential energy function embodied by the basis functions

$$\min f(p_{i1}) = \int (V_d(x) - V(x))^2 dx = \int (V_d(x) - \sum V_i(x))^2 dx. \tag{2.23}$$

subject to the constraint:

$$p_{i1} = 0, 1, 2, 3, 4, 5, 6, 7. \tag{2.24}$$

Because the basis functions are approximately local such that there is a small amount of overlap between adjacent basis functions, and almost no overlap between non-adjacent basis functions, we select an initial guess for $p_{i1}$ that results in $c_i = V_d(x = x_{0i})$, where the peaks of the basis function correspond to the value of the desired potential energy function at the peak position $x = x_{0i}$. This step is visualized in Fig. 2.3cd. In the special case where the basis functions are local and have no overlap, or the basis functions are local but

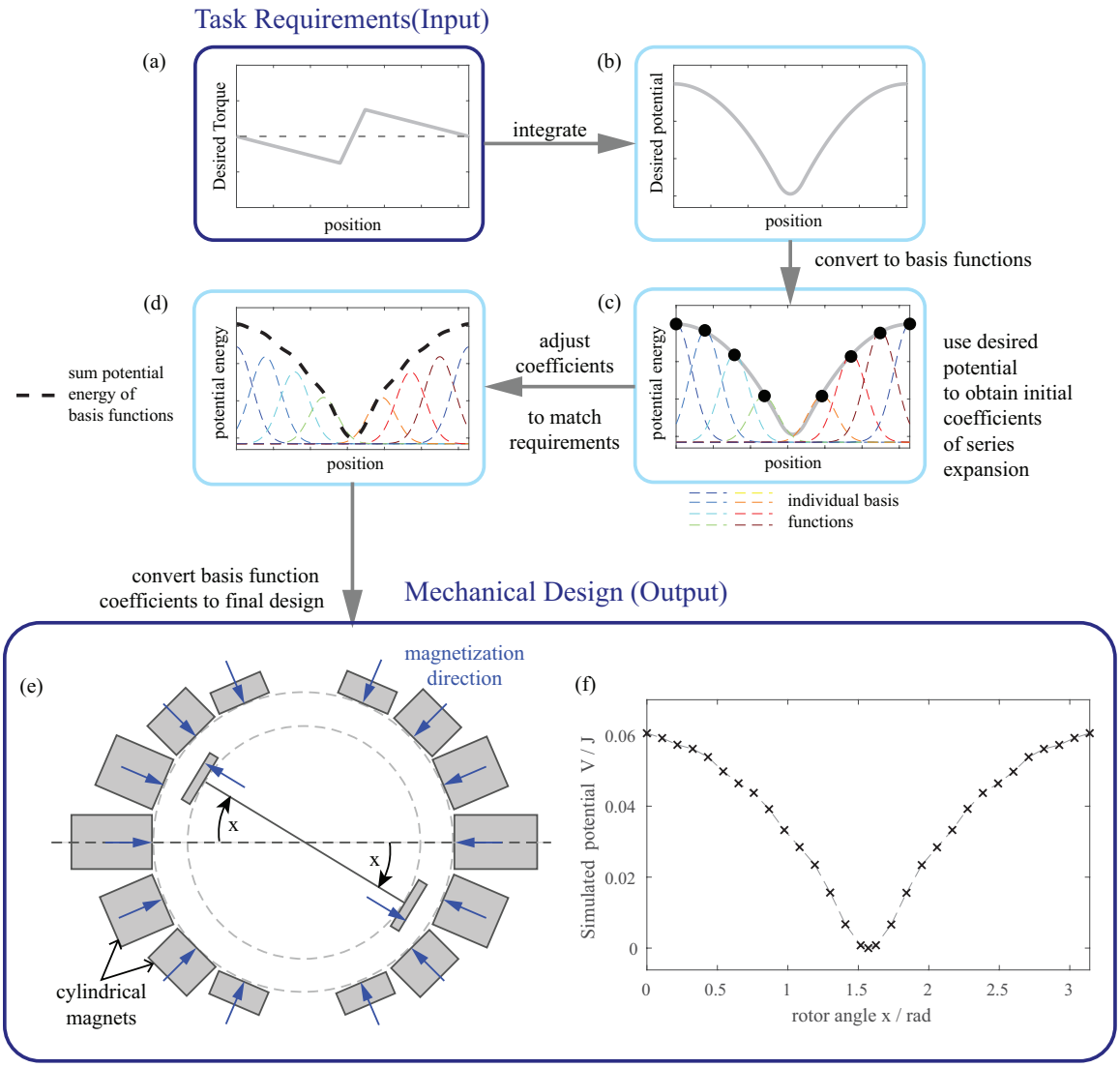


Figure 2.3: Design pipeline to make a spring which decreases torque the further away it is displaced from equilibrium. (a) Task requirements formulated in terms of desired torque function (grey). (b) Desired torque function integrated to obtain desired potential energy function (grey). (c) Attempting to decompose the desired potential energy function in terms of a series expansion of basis functions, where the initial guess for the coefficients of each basis function are obtained from the value of desired potential energy where the maximum value of each individual basis function is located. (d) Final potential energy obtained by optimizing basis function coefficients and summing the resulting series expansion (black dashed). Individual basis function contributions are shown in colored dashed lines. (e) Final mechanical design translated from basis functions in prior step. This final design is composed of cylindrical magnets arranged on a static ring of various lengths. The position coordinate $x$ in the basis functions corresponds to the angular position of two rotating magnets in the center of the ring of stationary magnets. Direction of magnetiziation of each magnet is indicated by the blue arrows, each magnet has a constant and uniform magnetization equal in magnitude to all other magnets. (f) Simulated potential energy function of the magnet configuration from (e). This plot was obtained by numerically simulating the magnetic field of the system in (e) using CST software, while sweeping the rotor angle $x$ from $[0, \pi]$.

overlap where one basis function is always 0 at the positions of the peaks of other basis functions, this kind of initial guess is equal to the optimal solution. We shall elaborate this point later in the discussion.

Using the final optimal $p_{i1}$:

$$p_{11} = 8, \quad p_{21} = p_{81} = 6, \quad p_{31} = p_{71} = 4, \quad p_{41} = p_{61} = 2, \quad p_{51} = 0. \tag{2.25}$$

we obtain a final design consisting of the number of stacked magnets in each location on the stator, shown in Fig. 2.3e from the top view, where the gray rectangles are stacked cylindrical magnets, the blue arrows indicate the direction of magnetization of each magnet, and $x$ is the rotation angle of the rotor magnets. Figure 2.3f. shows the numerically simulated potential energy function obtained using CST simulation software, which is similar to the desired potential energy function(grey) in Fig. 2.3b. and the approximate potential energy function obtained by optimizing the coefficients of the basis functions(black dashed line) in Fig. 2.3d.

(ii) Design problem 2: Spring with three equilibrium positions of equal potential energy.

This design problem is to make a spring with three stable equilibrium positions, where each position has the same potential energy as the others. We shall follow the same procedure detailed in the previous design problem, where we first describe a desired torque function which fulfills the task requirements

$$\tau_d(x) = \begin{cases} 0.443x & \text{if} \quad 0 < x \leq \frac{\pi}{16} \\ 0.087 & \text{if} \quad \frac{\pi}{16} < x \leq \frac{3\pi}{16} \\ -0.443x + 0.348 & \text{if} \quad \frac{3\pi}{16} < x \leq \frac{5\pi}{16} \\ -0.087 & \text{if} \quad \frac{5\pi}{16} < x \leq \frac{7\pi}{16} \\ 0.443x - 0.696 & \text{if} \quad \frac{7\pi}{16} < x \leq \frac{9\pi}{16} \\ 0.087 & \text{if} \quad \frac{9\pi}{16} < x \leq \frac{11\pi}{16} \\ -0.443x + 1.04 & \text{if} \quad \frac{11\pi}{16} < x \leq \frac{13\pi}{16} \\ -0.087 & \text{if} \quad \frac{13\pi}{16} < x \leq \frac{15\pi}{16} \\ 0.443x - 1.39 & \text{if} \quad \frac{15\pi}{16} < x \leq \pi. \end{cases} \tag{2.26}$$

Figure 2.4a. plots the desired torque (grey) from (2.26), and the torque approximated by the basis functions (black dashed), and the individual basis functions that make up the final approximated torque (colored dashed). Figure 2.4b. shows the resulting magnet configuration (top view) that embodies the final torque-deflection curve (black dashed) in Fig. 2.4a., where $x$ is the rotation angle of the inner magnets which make

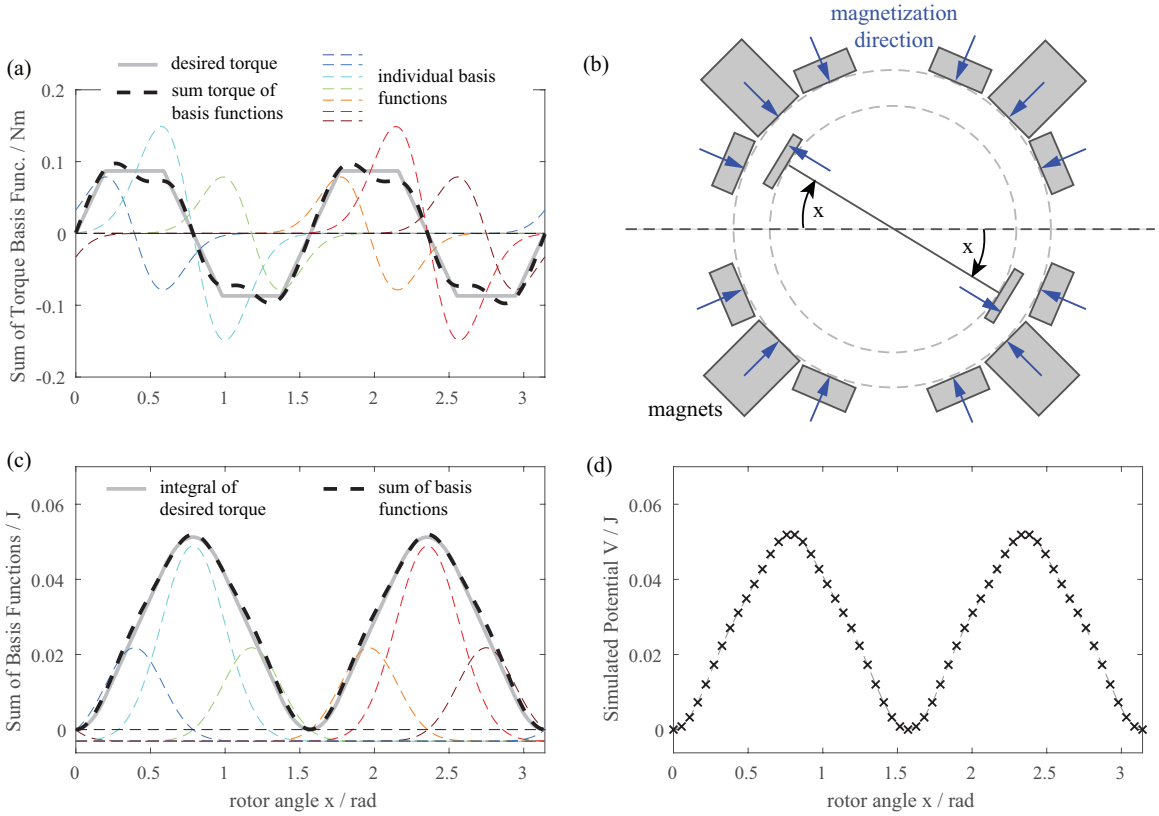


Figure 2.4: Design problem for a spring with three equilibrium lengths of equal potential energy, and the resulting basis function solution and final mechanical design. (a) Torque versus rotor angle $x$ plot of desired torque (grey), approximation using basis functions(black dashed), and individual basis functions in approximation (colored dashed). (b) Resulting magnetic configuration of final mechanism design. Grey rectangles are the top view of cylindrical magnets, while blue arrows indicate direction of magnetization. Each magnet has the same magnitude of magnetization, but with different directions. $x$ indicates the rotation angle of the center magnets, which are movable. (c) Potential energy vs. rotor angle $x$ of the integral of the desired torque (grey), the sum of the basis functions to approximate the integral of desired torque (black dashed), and the individual basis functions (colored dashed). (d) Simulation results of the potential energy vs. rotor angle $x$ of the magnet configuration in (b) found using CST software.

up the rotor.

We can then integrate the desired torque in (2.26) to obtain a desired potential energy function, given by

$$V_d(x) = \begin{cases} 0.222x^2 & \text{if} \quad 0 < x \leq \frac{\pi}{16} \\ 0.087x - 0.00854 & \text{if} \quad \frac{\pi}{16} < x \leq \frac{3\pi}{16} \\ -0.222x^2 + 0.348x - 0.0854 & \text{if} \quad \frac{3\pi}{16} < x \leq \frac{5\pi}{16} \\ -0.087x + 0.128 & \text{if} \quad \frac{5\pi}{16} < x \leq \frac{7\pi}{16} \\ 0.222x^2 - 0.696x + 0.547 & \text{if} \quad \frac{7\pi}{16} < x \leq \frac{9\pi}{16} \\ 0.087x + -0.145 & \text{if} \quad \frac{9\pi}{16} < x \leq \frac{11\pi}{16} \\ -0.222x^2 + 1.04x - 1.18 & \text{if} \quad \frac{11\pi}{16} < x \leq \frac{13\pi}{16} \\ -0.087x + 0.265 & \text{if} \quad \frac{13\pi}{16} < x \leq \frac{15\pi}{16} \\ 0.222x^2 - 1.39x + 2.18 & \text{if} \quad \frac{15\pi}{16} < x \leq \pi. \end{cases} \tag{2.27}$$

Figure 2.4c. plots the desired potential energy (grey) from (2.27), the potential energy approximated by the sum of the basis functions (black dashed line), and the potential energy of the individual basis functions (colored dashed lines). Figure 2.4d. plots the potential energy function obtained through numerical simulation in CST software.

(iii) Design problem 3: Spring with three different equilibrium positions with different potential energies.

In this problem, we would like a spring with three local minima such that we can use a torque to store energy inside the spring, but retain this potential energy after removing the applied torque, therefore making this a ”self-locking” spring.

The desired torque which satisfies the design requirements is:

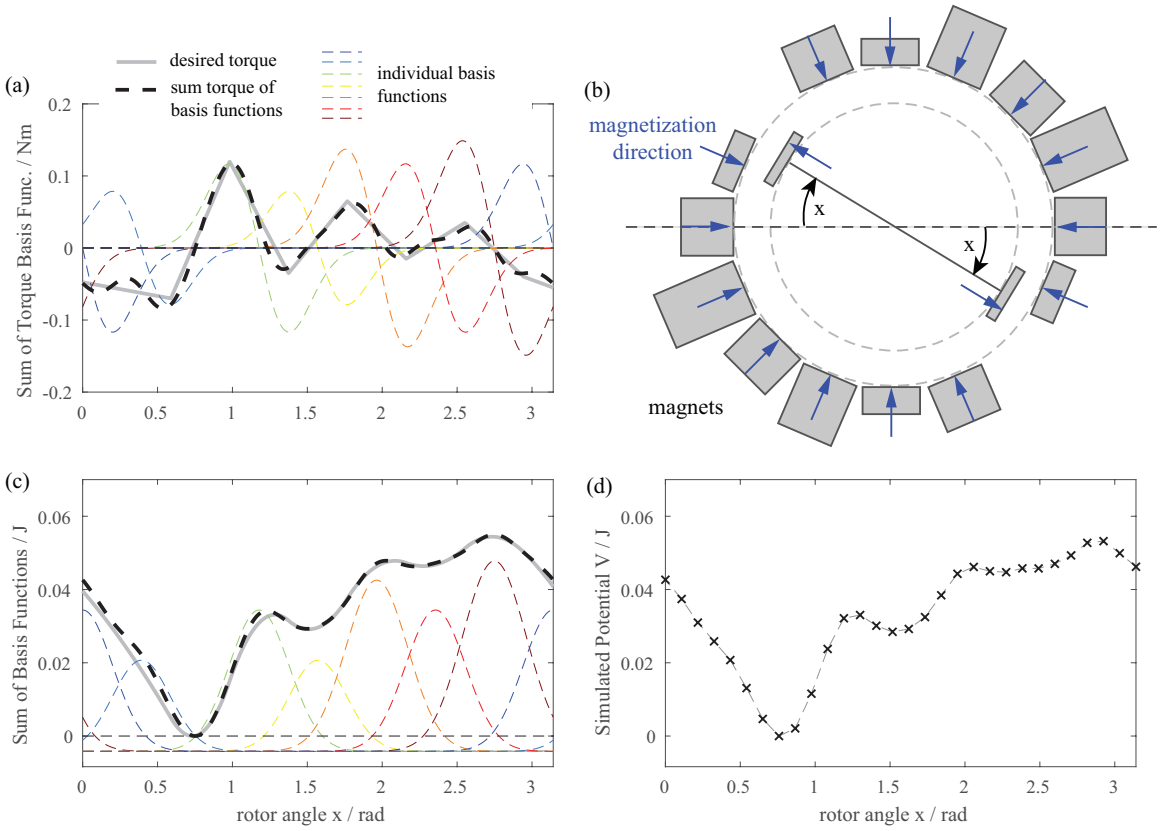


Figure 2.5: Design problem for a spring with three equilibrium lengths of different potential energy, and the resulting basis function solution and final mechanical design. (a) Torque vs. rotor angle $x$ plot of desired torque(grey), approximation using basis functions(black dashed), and individual basis functions in approximation(colored dashed). (b) Resulting magnetic configuration of final mechanism design. Grey rectangles are the top view of cylindrical magnets, while blue arrows indicate direction of magnetization. Each magnet has the same magnitude of magnetization, but with different directions. $x$ indicates the rotation angle of the center magnets, which are movable. (c) Potential energy vs. rotor angle $x$ of the integral of the desired torque(grey), the sum of the basis functions to approximate the integral of desired torque(black dashed), and the individual basis functions(colored dashed). (d) Simulation results of the potential energy vs. rotor angle $x$ of the magnet configuration in (b) found using CST software.

$$\tau_d(x) = \begin{cases} -0.0475 - 0.0382x & \text{if} \quad 0 < x \leq \frac{3\pi}{16} \\ -0.355 + 0.484x & \text{if} \quad \frac{3\pi}{16} < x \leq \frac{5\pi}{16} \\ 0.508 - 0.395x & \text{if} \quad \frac{5\pi}{16} < x \leq \frac{7\pi}{16} \\ -0.385 + 0.255x & \text{if} \quad \frac{7\pi}{16} < x \leq \frac{9\pi}{16} \\ 0.425 - 0.204x & \text{if} \quad \frac{9\pi}{16} < x \leq \frac{11\pi}{16} \\ -0.29 + 0.127x & \text{if} \quad \frac{11\pi}{16} < x \leq \frac{13\pi}{16} \\ 0.523 - 0.191x & \text{if} \quad \frac{13\pi}{16} < x \leq \frac{15\pi}{16} \\ 0.185 - 0.0764x & \text{if} \quad \frac{15\pi}{16} < x \leq \pi. \end{cases} \tag{2.28}$$

Figure 2.5a. plots the desired torque (grey) from (2.28), the approximated torque using the basis functions (black dashed), and the individual basis functions (colored dashed lines). Figure 2.5b. shows the magnet configuration used to embody the task requirements. We can integrate the desired torque in (2.28) to obtain the desired potential energy:

$$V_d(x) = \begin{cases} -0.0191x^2 - 0.0475x - 0.0223 & \text{if} \quad 0 < x \leq \frac{3\pi}{16} \\ 0.242x^2 - 0.355x + 0.0682 & \text{if} \quad \frac{3\pi}{16} < x \leq \frac{5\pi}{16} \\ -0.197x^2 + 0.508x - 0.355 & \text{if} \quad \frac{5\pi}{16} < x \leq \frac{7\pi}{16} \\ 0.127x^2 - 0.385x + 0.258 & \text{if} \quad \frac{7\pi}{16} < x \leq \frac{9\pi}{16} \\ -0.102x^2 + 0.425x - 0.458 & \text{if} \quad \frac{9\pi}{16} < x \leq \frac{11\pi}{16} \\ 0.0637x^2 - 0.29x + 0.315 & \text{if} \quad \frac{11\pi}{16} < x \leq \frac{13\pi}{16} \\ -0.0955x^2 + 0.523x - 0.722 & \text{if} \quad \frac{13\pi}{16} < x \leq \frac{15\pi}{16} \\ -0.0382x^2 + 0.185x - 0.225 & \text{if} \quad \frac{15\pi}{16} < x \leq \pi. \end{cases} \tag{2.29}$$

Figure 2.5c. shows the desired potential energy (grey) in (2.29) offset such that the minimum potential energy is at $V = 0$, the approximated potential energy using the basis functions (black dashed), and the individual basis functions (colored dashed). Figure 2.5d. plots the numerically simulated potential energy function using the magnet configuration in Fig. 2.5b.

In the next section, we shall demonstrate an experimental prototype to realize the set of 1-degree-of-freedom basis functions proposed in this section. We then reconfigure the prototype to solve the three design problems shown in this section, and characterize the torque-deflection data.

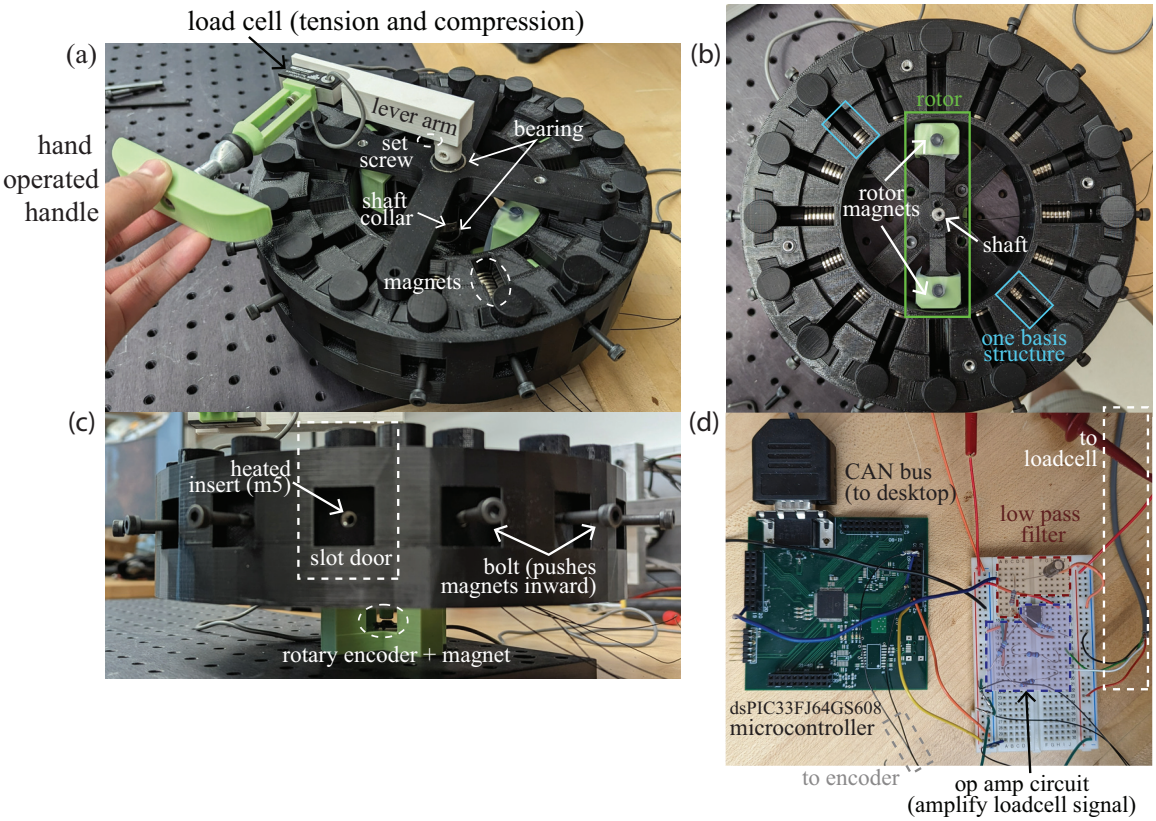


Figure 2.6: Adjustable spring mechanism made from eight 1-degree-of-freedom basis structures connected in parallel. (a,b,c) The spring consists of a rotor with magnets on both sides, and a cylindrical stator consisting of 16 magnet slots, i.e an individual basis structure, which can be reconfigured to vary the number of magnets to scale/shift the individual basis potential energy function. The torque-deflection of the spring is obtained by attaching a lever arm to the rotor via a set-srew attachment to the rotating shaft, and pressing on a loadcell attached to the lever arm to get force data, and using a magnetic rotary encoder to obtain position data. Because the stator magnets repel the rotor magnets, a slot door with m5 heated inserts and bolts are used to press the magnets inwards so they remain stationary. (d) Electronics used to process sensor data. An op-amp circuit and a low pass filter (resistor and capacitor) are used to amplify the loadcell signal and filter for noise, respectively, before the voltage is read by a microcontroller and sent to a desktop computer running simulink realtime.

## 2.5 Experimental Validation

Figure. 2.6 shows the experimental prototype used to realize the 1-degree-of-freedom basis functions and the solutions to the design problems in the prior section. Figure 2.6ab. shows the mechanical prototype, which consists of a single rotor with two magnets on each side, and a surrounding stator consisting of 16 possible locations to stack a re-configurable number of magnets. The magnets in the stator are required to be symmetric, such that the positions on opposing ends of the ring have the same number of magnets. Therefore, the domain of the rotor position ranges from $\theta \in [0, \pi]$ or 0 to 180 degrees. Moreover, we note it is not possible to measure potential energy directly, only changes in potential energy, which can be done by measuring and integrating torque along the distance it is applied. Consequently, in Fig. 2.6a. there is a hand-operated load cell (Transducer Techniques MLP-10) attached to a lever arm connected to the rotor shaft to measure the torque applied to the rotor, and a magnetic rotary encoder to measure position data shown in Fig. 2.6c. Figure 2.6d. shows the electronics used to process and send the torque-deflection data to a desktop computer. We used an op amp circuit to first amplify the loadcell voltage, then an analog low pass filter (2200$\Omega$ resistor and $4.7k\mu F$ capacitor in series) to remove noise. Then we use a microcontroller (dspic33fj64gs608) to process the encoder data and measure the analog voltage of the loadcell after amplification and filtering, and use a CAN bus to send both the load cell and encoder data to a desktop computer running MATLAB's simulink realtime to plot and record the torque and position data to a text file.

Figure 2.7a. shows the experimentally obtained torque-deflection data for a single basis function, where 6 trials (grey) of experimental data were averaged to obtain the final result (blue) and the fitted Gaussian derivative torque-deflection curve (black dashed). Figure 2.7b. shows the integrated potential energy functions obtained from the experimentally collected torque-deflection functions (grey), and the integral of the average torque-deflection function(blue), and the fitted Gaussian function (black dashed) in Fig. 2.7a. It is here where we use the maximum of the fitted Gaussian function with respect to potential energy to back-calculate the correct magnetization (0.895 Wb) for the magnetostatic simulations running in CST software. Although the integral of the individual torque-deflection functions (grey) deviate significantly from the predicted Gaussian potential functions, the average of these curves(blue) shows close agreement with a Gaussian potential function. This is to be expected since there is unavoidable noise in the loadcell used to measure torque, and that potential energy cannot be measured directly thereby the integral of torque is only an indirect measurement.

Next we configured the magnets in the 1-degree-of-freedom mechanism for three different tasks, i) a spring which exerts a torque that decreases as the deflection is increased, ii) a spring with three stable equilibrium lengths which have identical potential energy values, and iii) a spring with three different stable equilibrium lengths which have different potential energy values at each equilibrium length. The configura-

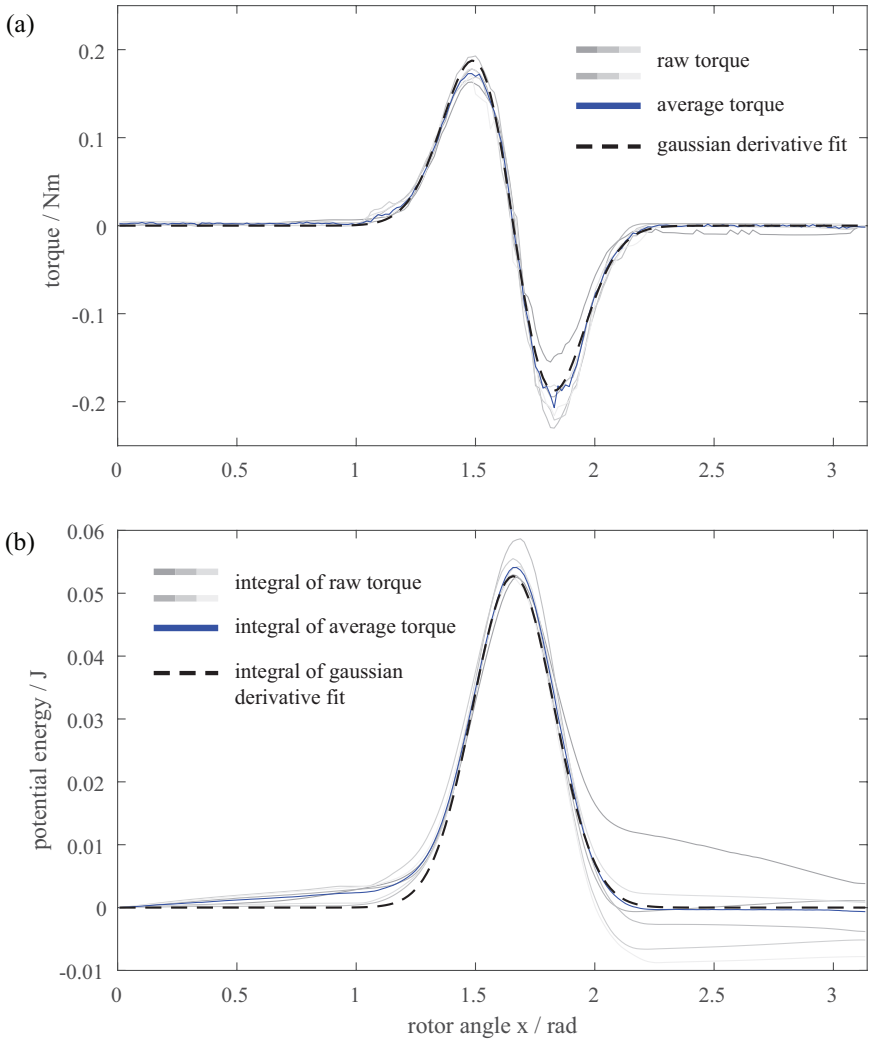


Figure 2.7: Experimental data obtained of a single basis function. (a) Torque vs. rotor angle $x$ of 6 experimental trials (grey), the average of the experimental trials (blue), and the fitted Gaussian derivative function with respect to the average (black dashed). (b) Potential energy vs. rotor angle $x$ of the integral of 6 experimentally obtained torque-deflection curves (grey), the average of the 6 integrated torque-deflection curves (blue), and the fitted Gaussian potential function (black dashed).

| description | Task 1 | Task 2 | Task 3 |
|---|---|---|---|
| $N$ of basis structure 1 | 8 | 0 | 4 |
| $N$ of basis structure 2 | 6 | 2 | 2 |
| $N$ of basis structure 3 | 4 | 8 | 0 |
| $N$ of basis structure 4 | 2 | 2 | 4 |
| $N$ of basis structure 5 | 0 | 0 | 2 |
| $N$ of basis structure 6 | 2 | 2 | 6 |
| $N$ of basis structure 7 | 4 | 8 | 4 |
| $N$ of basis structure 8 | 6 | 2 | 8 |

Table 2.2: Number of magnets used to construct each individual basis structure for each task. Each basis structure possesses a symmetric distribution of magnets, with half the magnets being placed on each of the two opposite ends of the stator, respectively.

tion of the number of $N$ stacked magnets in each basis function position for each different task are shown in Table 2.2.

Figure 2.8a. shows the magnet configuration for a task designed to decrease torque the further the position is from the equilibrium length, and labels the magnet positions corresponding to the peak of each potential energy basis function. Figure 2.8b. shows the experimentally obtained torque-deflection plots (grey lines), and the average of the 6 experiment plots (blue). The torque-deflections were obtained by pushing/pulling on the loadcell of the lever arm to move the rotor at a rate of half a revolution per minute, or 0.0083 Hz. In addition to the low pass filter used to reduce noise in the loadcell, to remove the effect of inertial or damping forces on the loadcell, three of the six torque-deflection plots were obtained by moving rotor from 0 to $\pi$ radians, and the other three curves were obtained by moving the rotor in the opposite direction from $\pi$ to 0 radians. In order to mitigate noise and later obtain a conservative potential energy function $V(0) = V(\pi)$, we fit the sum of eight Gaussian derivative functions (black dashed line) to the average of the torque-deflection plots, where we assume this curve is symmetric about approximately $\theta = \pi/2$. Figure 2.8c. shows the individual Gaussian derivative functions (colored dashed lines) which make up the fitted torque-deflection curve (black dashed). Here we have assumed that the amplitude of the fifth basis function is zero due to no magnets being placed at position 5. Figure 2.8d. shows the potential energy functions obtained by integrating the experimentally obtained torque-deflection curves (grey), the average of the 6 experiment plots (blue), and the integral of the fitted sum of Gaussian derivative curves (black dashed). Figure 2.8e. shows the individual Gaussian potential energy basis functions (colored dashed lines) which make up the integral of the fitted torque-deflection curve (black dashed).

Figure 2.9a. shows the magnet configuration for a task designed to create as spring with three equilibrium lengths of equal potential energy. Figure 2.9b. shows the experimentally obtained torque-deflection plots (grey lines), the average of the 6 experiment plots (blue), and the curve obtained by fitting eight Gaussian

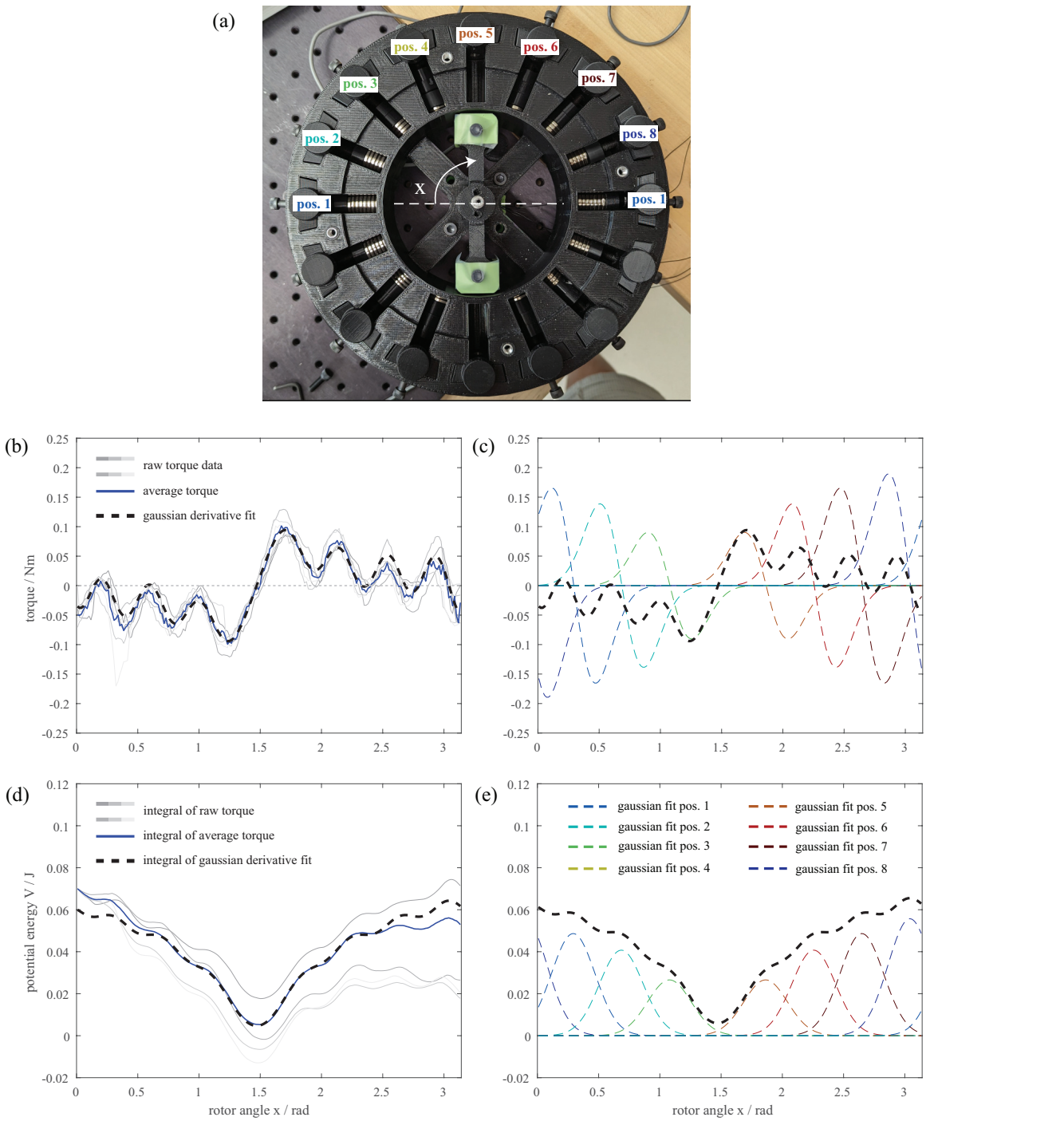


Figure 2.8: Experimental setup for a 1-degree-of-freedom spring with magnets configured for a torque-deflection curve which decreases absolute torque as the distance from the equilibrium length increases. (a) Overhead view showing configuration of magnets and position of the rotor $\theta$. There are 8 positions which form the centers of the Gaussian potential basis functions, labeled "pos. 1" up to "pos. 8." (b) Measured torque-deflection curve, raw data(grey lines), average of raw data (blue line), sum of Gaussian fitted curves (black dashed line). (c) Torque-deflection curves of each individual Gaussian derivative curve (colored lines) in the fitted curve (black dashed line). (d) Potential energy function obtained from integrating measured(grey lines), integral of the average of measured torque(blue line), and integral of the fitted torque deflection curve(black dashed line). (e) Potential energy curves of each individual Gaussian curve (colored lines) in the fitted curve (black dashed line). These are the basis functions obtained by fitting to experimental data.

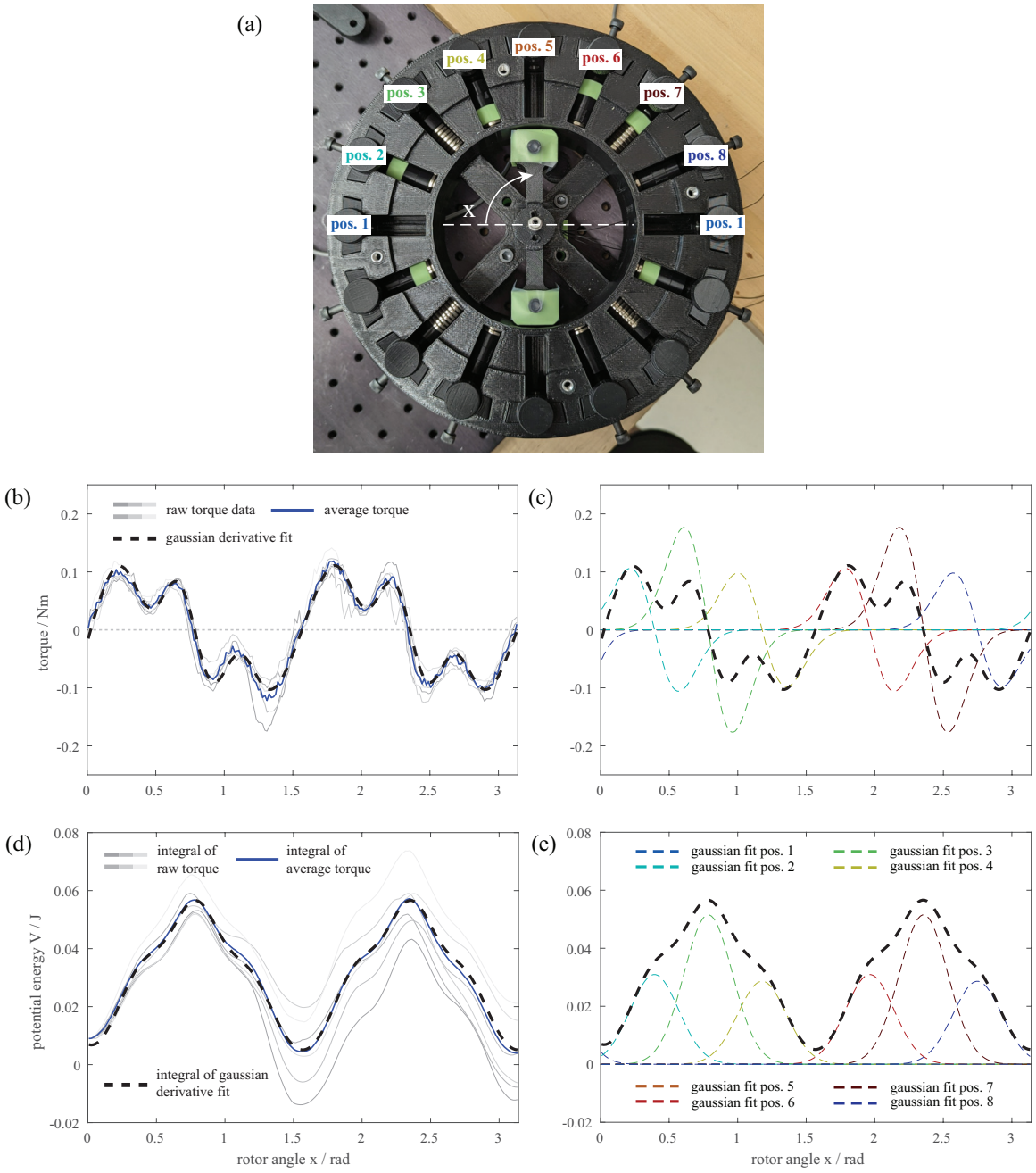


Figure 2.9: Experimental setup for a 1-degree-of-freedom spring with magnets configured for a torque deflection curve with three equilibrium lengths of equal potential energy. (a) Overhead view showing magnet configuration There are 8 positions which form the centers of the Gaussian potential basis functions, labeled "pos. 1" up to "pos. 8." (b) Measured torque-deflection curve, raw data (grey lines), average of raw data (blue line), sum of Gaussian fitted curves (black dashed line). (c) Torque-deflection curves of each individual Gaussian derivative curve (colored lines) in the fitted curve (black dashed line). (d) Potential energy function obtained from integrating measured (grey lines), integral of the average of measured torque(blue line), and integral of the fitted torque deflection curve (black dashed line). (e) Potential energy curves of each individual Gaussian curve (colored lines) in the fitted curve (black dashed line). These are the basis functions obtained by fitting to experimental data.

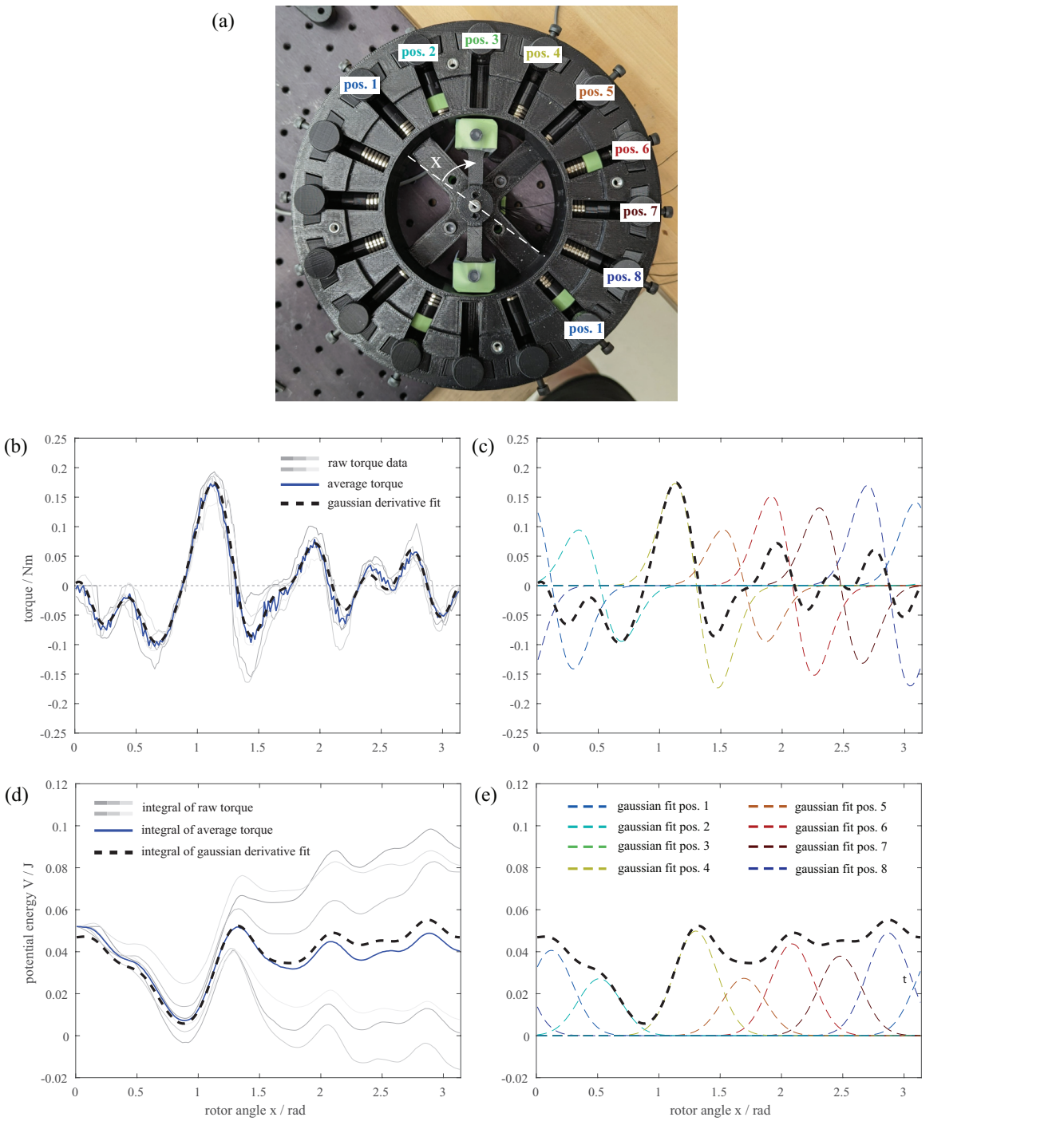


Figure 2.10: Experimental setup for a 1-degree-of-freedom spring with magnets configured for a torque deflection curve with three equilibrium lengths of different potential energies. (a) Overhead view showing magnet configuration There are 8 positions which form the centers of the Gaussian potential basis functions, labeled "pos. 1" up to "pos. 8." (b) Measured torque-deflection curve, raw data (grey lines), average of raw data (blue line), sum of Gaussian fitted curves (black dashed line). (c) Torque-deflection curves of each individual Gaussian derivative curve (colored lines) in the fitted curve (black dashed line). (d) Potential energy function obtained from integrating measured(grey lines), integral of the average of measured torque(blue line), and integral of the fitted torque deflection curve(black dashed line). (e) Potential energy curves of each individual Gaussian curve (colored lines) in the fitted curve (black dashed line). These are the basis functions obtained by fitting to experimental data.

derivative functions to the average of the torque-deflection data (black-dashed). Figure 2.9c. shows the individual Gaussian derivative functions (colored lines) which make up the fitted torque-deflection curve (black dashed). Here we have assumed that basis functions 1, 5, and 8 are 0 due to no magnets being placed in those positions. Figure 2.9d. shows the potential energy functions obtained by integrating the experimentally obtained torque-deflection curves (grey), the average of the 6 experiment plots (blue), and the integral of the fitted sum of Gaussian derivative curves (black dashed line). Figure 2.9e. shows the individual Gaussian potential energy basis functions (colored lines) which make up the integral of the fitted torque-deflection curve (black dashed line).

Figure 2.10a. shows the magnet configuration for a task designed to create as spring with three equilibrium lengths of increasing potential energy. Figure 2.10b. shows the experimentally obtained torque-deflection plots(grey), the average of the 6 experiment plots(blue), and the curve obtained by fitting eight Gaussian derivative functions to the average of the torque-deflection data (black-dashed). Figure 2.10c. shows the individual Gaussian derivative functions(colored lines) which make up the fitted torque-deflection curve (black dashed). Here we have assumed that basis function 3 is 0 due to no magnets being placed in this position. Figure 2.10d. shows the potential energy functions obtained by integrating the experimentally obtained torque-deflection curves (grey), the average of the 6 experiment plots (blue), and the integral of the fitted sum of Gaussian derivative curves (black dashed). Figure 2.10e. shows the individual Gaussian potential energy basis functions (colored lines) which make up the integral of the fitted torque-deflection curve (black dashed line).

### 2.6 Discussion and Conclusion

In this paper, we have discussed an analytical method of automatic design by exploiting approximation theory. In the field of automatic design, topology optimization is the current-state-of-the-art. Although a powerful tool, topology optimization requires extensive numerical computation. In this paper, we have provided a way to directly reach the desired mechanical design using approximation and analytical calculation. The main analytical calculation to determine the design parameters using (2.16) is simplified compared to a large scale optimization due to the locality of the basis functions. In particular, due to the locality of the basis functions, the value of the potential energy in a specific subdomain of one basis function can be varied by altering the physical dimension in the corresponding basis structure, and not the other basis structures whose basis function domains do not overlap. This feature was used to simplify the design problem considered in this paper.

Despite the usefulness of a simple analytical calculation exploiting approximation theory and orthogonality of basis functions in a series expansion, the main bottleneck of this method is in the design of the basis

structures themselves. Although basis structures with completeness guarantee any potential energy function and therefore task can be approximated, design problems have other requirements such as maximum weight, portability, and manufacturability, which the proposed basis structures may not be ideal for compared to basis functions that do not guarantee completeness. For example, the spring-like mechanisms realized for the design problems in the preceding section can store at most 0.06 J of energy while the entire prototype excluding the sensor electronics and reconfigurable number of magnets weighs 2.03 kg, giving a total energy density of 0.03 J/kg. A typical commercially available steel coil-spring which typically possesses a linear torque-deflection curve, possesses an energy density between $50 - 100$ J/kg. Formulating and solving a design problem to include other constraints besides torque-deflection characteristics represents a logical next step for this research. Additionally, topology optimization may be used to find better optimized basis structures which take into account other constraints. The optimized basis structure could be reused to design different mechanisms, rather than formulating and solving a new topology optimization problem for different mechanisms.

The primary use of a method to design passive devices with arbitrary potential energy functions is to create multistable mechanisms, which have a variety of applications [26, 27, 28, 29], such as shape-changing [30, 31], storing and releasing energy, or improving energy efficiency of actuators [32]. Given the usefulness of multi-stable mechanisms, there are some design methods to customize the potential energy function to be multi-stable using known building blocks. A common building block is a bistable curved beam, however there are other building blocks such as perforated shells [33, 34], origami structures [35], composites, or even magnetic torsion springs [36, 37, 38, 39]. Although these building blocks and associated optimization/deep learning methods [40, 34, 41] are useful to design multi-stable systems with more than one equilibrium configuration, the potential energy function of each building block design by these methods does not guarantee a solution for an arbitrary desired torque-deflection curve characterizing the multistable system. However, these optimization/deep-learning methods can incorporate additional constraints (e.g weight, size, portability) in addition to completing the task. Perhaps a combination of optimization/deep learning methods with analytical methods can be used to find and guarantee a solution which can perform the task in less time, whilst also incorporating a variety of design constraints.

The analytical design method described in this paper provides a way to design complex passive mechanisms. Current passive-mechanisms are relatively simple and limited to levers to amplify mechanical advantage, or springs with linear force-deflection profiles to store and recycle energy. In the prior sections, we described how to design more complex force-deflection curves for 1-degree-of-freedom passive mechanisms. Here we shall talk about the applications of these more complicated force-deflection curves in greater detail.

In the first design problem of the prior section, we described how to design a spring which exerts a torque

that decreases as it is deflected further from the equilibrium position. An application of such a spring is to attach this spring in parallel with a human leg to minimize the force required to support the human during a walking task. In order to minimize the force required to support the body during walking, ideally we want to minimize the force in the vertical direction, such that the body does not move at all in the vertical direction, and maximize force in the horizontal direction. This can be done when the force in the vertical direction is equal to and opposite to the gravitational force on the point-mass, even when the body is moving horizontally. In particular, when the center of mass of the human body moves in a straight line in legged movement, the force exerted on the human is minimized because there is no vertical momentum which must be redirected in each step, therefore only the minimum force to support the body-weight is needed in the vertical direction. In running or walking where there is vertical momentum to redirect, the vertical force required to sustain this motion is equal to the weight of the body and the inertial force from the acceleration of the body upwards during redirection. Consequently, reducing the force requirements by enabling straight-line motion would lower the material strength requirements of an exoskeleton to allow passive walking [3], therefore potentially lowering the mass of such an exoskeleton. A suitable force-deflection characteristic of a spring attached to the leg for this type of motion is

$$F(\Delta l) = \frac{Mg}{y}(l_0 - \Delta l), \tag{2.30}$$

where $M$ is the total mass of the human, assumed to be concentrated at the center of mass, $g$ is the gravitational acceleration, $y$ is the height of the center of mass relative to the ground, and $l_0$ is the maximum length of the exoskeleton. This force-deflection profile has a maximum force at $\Delta l = 0$, which decreases linearly as $\Delta l$ increases. Although the mechanism described in the prior section was a rotating torsional spring, this can be converted into an axial spring by using a ballscrew system, therefore turning the mechanism in the first design problem into an axial spring which supplies a decreasing force as the deflection is increased to fulfill this task (2.30). This illustrative example shows that minimizing the total force on the body in legged locomotion may be achieved by a spring leg with an unusual force-deflection curve designed using the method proposed in this paper.

In the second design problem, we described how to design a spring with multiple equilibrium lengths of the same potential energy. This kind of device can be used to build structures that can transition to multiple shapes, but hold them stably without too much exerted force. For example, deployable structures are structures which fold into a smaller volume for portable transport, and can be deployed into a different shape, often larger, for practical use. These structures, which are often inspired by origami, have little assembly required because they are made of one single piece which can be folded into different shapes rather than separate pieces which must be glued/bolted together to maintain a solid structure. Examples are folding tents to

replace cloth tents [42], a twisting multistable ladder to make linearly compressible shapes [31], or actuators with bi-stable modes to reduce the energy cost of holding a position[26, 27, 29]. The main principle behind shape-changing objects is that the pre-programmed shapes are potential energy minima with respect to the positions of elements in the structure [20]. In order to transition between different shapes, one must apply a large force to overcome the potential energy barrier between shapes. But after the new shape is achieved, no additional force is required to maintain this shape because it is a stable equilibrium.

In the third design problem, we described how to design a spring with multiple equilibrium lengths, with different potential energies. In this case, we can store potential energy inside a spring, remove the force used to do work to supply the energy, but still retain that energy inside the spring. This energy can be left undisturbed inside the spring for any amount of time because the potential energy has a local minima, and then when that energy is needed, we can provide a small amount of force to get over the nearby potential energy barrier, after which the spring will enter an unstable equilibrium and release the energy automatically. This type of spring may be useful to make built-in locking mechanisms for springs in applications where timed energy storage and release are essential. Examples are a task to lift heavy objects off the floor [43, 44]. For example, this may be done using a springy exoskeleton which allows a human to squat to store energy inside the spring, hold that energy, pick up an object, then adjust the stiffness of the exoskeleton to increase the force it uses to release the energy. As a result, a human can lift heavier weights than they are typically capable of, whilst still being solely responsible for supplying the energy, and therefore only requiring a passive mechanism for assistance. However, the process of holding energy inside the spring and adjusting stiffness of a spring requires a locking mechanism to lower the energy cost of changing stiffness, and to prevent energy from being released before it is required. Otherwise, a motor would be required to supply a force to oppose the spring from releasing energy, which costs energy to operate. Locking mechanisms typically add extra bulk for achieving some energy cost savings. However, if the spring was designed with a special force-deflection characteristic which possessed local minima of different potential energy, then it would be inherently self-locking, which may simplify the design of passive mechanisms to achieve timed energy storage and release.

## References


[1] S. M. Felton, D.-Y. Lee, K.-J. Cho, and R. J. Wood, "A passive, origami-inspired, continuously variable transmission," *IEEE ICRA 2014*, vol. 1, pp. 2913–2918, 2014.

[2] C. M. Thompson and M. H. Raibert, "Passive dynamic running," *Experimental Robotics*, vol. 1, pp. 74–83, 1990.

[3] T. McGeer, "Passive dynamic walking," *Int. J. Robot. Res.*, vol. 9, no. 2, pp. 62–82, 1990.

[4] S. Collins, A. Ruina, R. Tedrake, and M. Wisse, "Efficient bipedal robots based on passive-dynamic walkers," *Science*, vol. 307, no. 5712, pp. 1082–1085, 2005.

[5] A. Sutrisno and D. J. Braun, "Enhancing mobility with quasi-passive variable stiffness exoskeletons," *IEEE T. Neural Syst. Rehabil. Eng.*, vol. 27, no. 3, pp. 487–496, 2019.

[6] ——, "How to run 50% faster without external energy," *Sci. Adv.*, vol. 6, no. 13, p. eaay1950, 2020.

[7] E. W. Hawkes, C. Xiao, R.-A. Peloquin, C. Keeley, M. R. Begley, M. T. Pope, and G. Niemeyer, "Engineered jumpers overcome biological limits via work multiplication," *Nature*, vol. 604, p. 657, 2022.

[8] J. L. Silverberg, A. A. Evans, L. McLeod, R. C. Hayward, T. Hull, C. D. Santangelo, and I. Cohen, "Using origami design principles to fold reprogrammable mechanical metamaterials," *Science*, vol. 345, p. 6197, 2014.

[9] J. T. B. Overvelde, T. A. de Jong, Y. Shevchenko, S. A. Becerra, G. M. Whitesides, J. C. Weaver, C. Hoberman, and K. Bertoldi, "A three-dimensional actuated origami-inspired transformable metamaterial with multiple degrees of freedom," *Nat. Comm.*, vol. 7, p. 10929, 2016.

[10] Y. Kim, H. Yuk, R. Zhao, S. A. Chester, and X. Zhao, "Printing ferromagnetic domains for unthethered fast-transforming soft materials," *Nature*, vol. 558, pp. 274–279, 2018.

[11] T. Chen, M. Pauly, and P. M. Reis, "A reprogrammable mechanical metamaterial with stable memory," *Nature*, vol. 589, p. 386, 2021.

[12] A. Pal, V. Restrepo, D. Goswami, and R. V. Martinez, "Exploiting mechanical instabilities in soft robotics: Control, sensing, and actuation," *Advanced Materials*, vol. 33, p. 2006939, 2021.

[13] A. Ion, L. Wall, R. Kovacs, and P. Baudisch, "Digital mechanical metamaterials," *CHI 2017*, vol. 1, pp. 977–988, 2017.

[14] Y. Song, R. M. Panas, S. Chizari, L. A. Shaw, J. A. Jackson, J. B. Hopkins, and A. J. Pascall, "Additively manufacturable micro-mechanical logic gates," *Nat. Comm.*, vol. 10, p. 882, 2019.

[15] C. Coulais, E. Teomy, K. de Reus, Y. Shokef, and M. van Hecke, "Combinatorial design of textured mechanical metamaterials," *Nature*, vol. 535, pp. 529–532, 2016.

[16] E. W. Hawkes and M. R. Cutkosky, "Design of materials and mechanisms for responsive robots," *Ann. Rev. Contr. Robot. Auton. Sys.*, vol. 1, pp. 359–384, 2018.

[17] M. P. Bendsoe and N. Kikuchi, "Generating optimal topologies in structural design using a homogenization method," *Comput. Methods Appl. Mech. Eng.*, vol. 71, p. 197, 1988.

[18] O. Sigmund and K. Maute, "Topology optimization approaches a comparitive review," *Struct. Multidisc. Optim.*, vol. 48, pp. 1031–1055, 2013.

[19] H. Ronellenfitsch, N. Stoop, J. Yu, A. Forrow, and J. Dunkel, "Inverse design of discrete mechanical metamaterials," *Physical Review Materials*, vol. 3, p. 095201, 2019.

[20] A. Iniguez-Rabago, Y. Li, and J. T. B. Overvelde, "Exploring multistability in prismatic metamaterial-sthrough local actuation," *Nat. Comm.*, vol. 10, p. 5577, 2019.

[21] B. Zhu, X. Zhang, H. Zhang, J. Liang, H. Zang, H. Li, and R. Wang, "Design of compliant mechanisms using continuum topology optimization: A review," *Mechanism and Machine Theory*, vol. 143, p. 103622, 2020.

[22] H. Lipson and J. B. Pollack, "Automatic design and manufacture of robotic lifeforms," *Nature*, vol. 406, pp. 974–978, 2000.

[23] S. Ha, S. Coros, A. Alspach, J. M. Bern, J. Kim, and K. Yamane, "Computational design of robotic devices from high-level motion specifications," *IEEE T. Robot.*, vol. 34, no. 5, pp. 1240–1251, 2018.

[24] V. Chalvet and D. J. Braun, "Algorithmic design of low-power variable-stiffness mechanisms," *IEEE T. Robot.*, vol. 33, pp. 1508–1515, 2017.

[25] S. Bonfanti, R. Guerra, F. Font-Clos, D. Rayneau-Kirkhope, and S. Zapperi, "Automatic design of mechanical metamaterial actuators," *Nat. Comm.*, vol. 11, p. 4162, 2020.

[26] A. Dahiya and D. J. Braun, "Efficiently tunable positive-negative stiffness actuator," *2017 IEEE Int. Conf. Rob. Autom.*, pp. 1235–1240, 2017.

[27] D. J. Braun, V. Chalvet, and A. Dahiya, "Positive-negative stiffness actuators," *IEEE T. Robot.*, vol. 35, no. 1, pp. 162–173, 2019.

[28] R. Zhang, T. Auzinger, and B. Bickel, "Computational design of planar multi-stable compliant structures," *ACM Trans. Graphics*, vol. 40, no. 5, p. 186, 2021.

[29] Y. Chi, Y. Li, Y. Zhao, Y. Hong, Y. Tang, and J. Yin, "Bistable and multistable actuators for soft robots: Structures, materials, and functionalities," *Adv. Mater.*, vol. 34, p. 2110384, 2022.

[30] G. Chen, S. Zhang, and G. Li, "Multistable behaviors of compliant sarrus mechanisms," *J. Mech. Robot.*, vol. 5, p. 021005, 2013.

[31] C. Aza, A. Pirrera, and M. Schenk, "Multistable morphing mechanisms of nonlinear springs," *J. Mech. Robot.*, vol. 11, p. 051014, 2019.

[32] L. Cappello, M. Xiloyannis, B. K. Dinh, A. Pirrera, F. Mattioni, and L. Masia, "Multistable series elastic actuators: Design and control," *Robot. Auton. Sys.*, vol. 118, pp. 167–178, 2019.

[33] J. Shi, H. Mofatteh, A. Mirabolghasemi, G. Desharnais, and A. Akbarzadeh, "Programmable multistable perforated shellular," *Adv. Mater.*, vol. 33, p. 2102423, 2021.

[34] Y. Wang, Q. Zeng, J. Wang, Y. Li, and D. Fang, "Inverse design of shell-based mechanical metamaterial with customized loading curves based on machine learning and genetic algorithm," *Comput. Methods Appl. Mech. Engrng.*, vol. 401, p. 115571, 2022.

[35] J. Kaufmann, P. Bhovad, and S. Li, "Harnessing the multistability of kresling origami for reconfigurable articulation in soft robotic arms," *Soft Robotics*, vol. 9, p. 212, 2022.

[36] A. Sudano, D. Accoto, L. Zollo, and E. Guglielmelli, "Design, development and scaling analysis of a variable stiffness magnetic torsion spring," *Int. J. Adv. Robot. Syst.*, vol. 10, p. 372:2013, 2013.

[37] B. Kozakiewicz and T. Winiarski, "Spring based on flat permanent magnets: Design, analysis and use in variable stiffness actuator," *Facta Universitatis*, vol. 21, p. 101, 2020.

[38] C. Forbrigger, A. Schonewille, and E. Diller, "Tailored magnetic torsion springs for miniature magnetic robots," *2021 IEEE Int. Conf. Robot. Autom.*, vol. 1, p. 7182, 2021.

[39] A. Seyedkanani and A. Akbarzadeh, "Magnetically assisted rotationally multistability metamaterials for tunable energy trapping-dissipation," *Adv. Func. Mater.*, vol. 32, p. 2207581, 2022.

[40] X. Zheng, T. te Chen, X. Guo, S. Samitsu, and I. Watanabe, "Controllable inverse design of auxetic metamaterials using deep learning," *Materials and Design*, vol. 211, p. 110178, 2021.

[41] Q. Zeng, Z. Zhao, H. Lei, and P. Wang, "A deep learning approach for inverse design of gradient mechanical metamaterials," *Int. J. Mech. Sci.*, vol. 240, p. 107920, 2023.

[42] D. Melancon, B. Gorissen, C. J. Garcia-Mora, C. Hoberman, and K. Bertoldi, "Multistable inflatable origami structures at the metre scale," *Nature*, vol. 592, p. 545, 2021.

[43] S. Y. Kim and D. J. Braun, "Novel variable stiffness spring mechanism: Modulating stiffness independent of the energy stored by the spring," *IEEE/RSJ Int. Conf. Int. Robots Sys.*, vol. 1, pp. 8232–8237, 2021.

[44] ——, "Variable stiffness floating spring leg: Performing net-zero energy cost tasks not achievable using fixed stiffness springs," *IEEE Robot. Autom. Lett.*, pp. 1–8, 2023.